Chapter 8
The Activity-Based Theoretical K–Ca and Na–Ca Geoindicators

Abstract Our activity-based theoretical K-Ca and Na-Ca geoindicators were tested with about one thousand reservoir liquids. The theoretical K-Ca geothermometers reproduce aquifer temperature with an average error of 3.8 °C and the error is lower than 10 °C in 97.3% of the cases. The theoretical Na-Ca geothermometers reproduce aquifer temperature with an average error of 6.9 °C and the error is less than 15 °C in 93.5% of the cases. The CO_2 fugacities given by our theoretical activity-based K-Ca and Na-Ca f_{CO_2}-indicators match the CO_2 fugacities given by the K-Ca f_{CO_2}-indicator of Giggenbach (1984), with an absolute deviation of 0.33 log-units on average, and reproduce the CO_2 fugacities given by speciation calculations, with an absolute deviation of 0.78 log-units on average. Furthermore, these theoretical K-Ca and Na-Ca geothermometers and f_{CO_2}-indicators allow one to identify the Ca-bearing solid phase in equilibrium with each reservoir liquid, either a Ca-Al-silicate (laumontite or clinozoisite or prehnite or wairakite) or calcite. This indication represents a substantial improvement with respect to the traditional K-Ca and Na-Ca geoindicators, is probably more reliable than the results of multicomponent chemical geothermometry, being slightly affected by pH and Al concentration, and may give qualitative clues on well permeability.

8.1 The K–Ca and Na–Ca Exchange Reactions and the Univariant Reactions Involving Calcite and a Ca–Al-Silicate

Under relatively low f_{CO_2} values, the K^2/Ca-activity ratio of reservoir liquids is probably controlled by equilibrium coexistence of hydrothermal minerals comprising a Ca–Al-silicate, adularia, a silica mineral and, in some cases, muscovite as well, as already recalled in Sect. 5.4.5. Plausible Ca–Al-silicates are laumontite [Lmt; $CaAl_2Si_4O_{12} \cdot 4H_2O$], clinozoisite [Czo; $Ca_2Al_3Si_3O_{12}(OH)$], prehnite [Prh; $Ca_2Al_2Si_3O_{10}(OH)_2$], and wairakite [Wrk; $CaAl_2Si_4O_{12} \cdot 2H_2O$]. They are involved in the K–Ca exchange reactions (5.131)–(5.134), which are rewritten and renumbered here for convenience:

$$2KAlSi_3O_8 + 4H_2O + Ca^{2+} = CaAl_2Si_4O_{12} \cdot 4H_2O + 2SiO_2 + 2K^+ \quad (8.1)$$

$$2.25KAlSi_3O_8 + 0.5H_2O + Ca^{2+} = 0.25KAl_3Si_3O_{10}(OH)_2$$
$$+ 0.5Ca_2Al_3Si_3O_{12}(OH) + 4.5SiO_2 + 2K^+ \quad (8.2)$$

$$2.5KAlSi_3O_8 + H_2O + Ca^{2+} = 0.5KAl_3Si_3O_{10}(OH)_2 + 0.5Ca_2Al_2Si_3O_{10}(OH)_2$$
$$+ 4.5SiO_2 + 2K^+ \quad (8.3)$$

$$2KAlSi_3O_8 + 2H_2O + Ca^{2+} = CaAl_2Si_4O_{12} \cdot 2H_2O + 2SiO_2 + 2K^+. \quad (8.4)$$
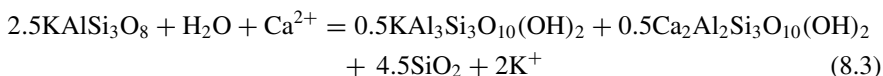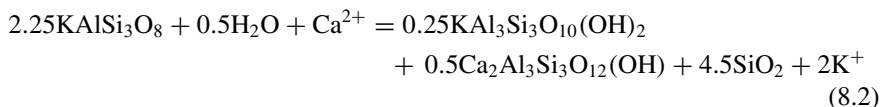
Likewise, under relatively low f_{CO_2} values, the Na^2/Ca-activity ratio is probably constrained by equilibrium coexistence of the same hydrothermal minerals either with albite *in lieu* of adularia, if muscovite is absent, or with albite *in lieu* of a part of adularia, if muscovite is present, as described by the Na–Ca exchange reactions (5.127)–(5.130), which are written again and renumbered here below:

$$2NaAlSi_3O_8 + 4H_2O + Ca^{2+} = CaAl_2Si_4O_{12} \cdot 4H_2O + 2SiO_2 + 2Na^+ \quad (8.5)$$

$$2NaAlSi_3O_8 + 0.25KAlSi_3O_8 + 0.5H_2O + Ca^{2+} = 0.25KAl_3Si_3O_{12}(OH)_2$$
$$+ 0.5Ca_2Al_3Si_3O_{12}(OH) + 4.5SiO_2 + 2Na^+ \quad (8.6)$$

$$2NaAlSi_3O_8 + 0.5KAlSi_3O_8 + H_2O + Ca^{2+} = 0.5KAl_3Si_3O_{12}(OH)_2$$
$$+ 0.5Ca_2Al_2Si_3O_{12}(OH)_2 + 4.5SiO_2 + 2Na^+ \quad (8.7)$$

$$2NaAlSi_3O_8 + 2H_2O + Ca^{2+} = CaAl_2Si_4O_{12} \cdot 2H_2O + 2SiO_2 + 2Na^+ \quad (8.8)$$
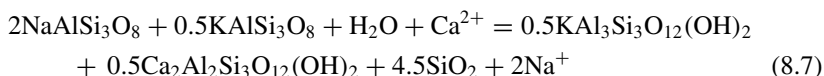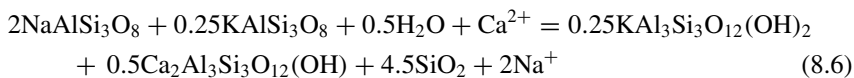
As already noted in Sect. 5.5, under relatively high f_{CO_2} values, the Ca–Al-silicates are not stable, and the K^2/Ca-activity ratio is probably governed by equilibrium coexistence of adularia, muscovite, a silica mineral, and calcite, according to reaction (5.139), which is rewritten and renumbered here under:

$$3KAlSi_3O_8 + CO_{2(g)} + Ca^{2+} + H_2O = CaCO_3 + KAl_3Si_3O_{12}(OH)_2$$
$$+ 6SiO_2 + 2K^+. \quad (8.9)$$
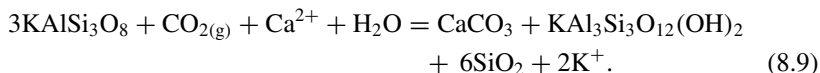
Reaction (8.9) represents the basis of the K–Ca f_{CO_2}-indicator of Giggenbach (1988). The Na^2/Ca activity ratio is probably controlled by a similar reaction, with albite *in lieu* of a part of adularia:

$$2NaAlSi_3O_8 + KAlSi_3O_8 + CO_{2(g)} + Ca^{2+} + H_2O = CaCO_3$$
$$+ KAl_3Si_3O_{12}(OH)_2 + 6SiO_2 + 2Na^+. \quad (8.10)$$
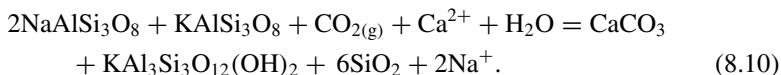
Reaction (8.10) represents the basis for a Na–Ca f_{CO_2}-indicator, which is derived in this book, following early suggestions of Ellis (1970) and Chiodini et al. (1991).

As already underscored in Sect. 5.5, equilibrium coexistence of calcite and a Ca–Al-silicate (either laumontite or clinozoisite or prehnite or wairakite), together with adularia, muscovite, and a silica mineral, acts as a CO_2 buffer (Giggenbach 1981, 1984, 1988; Arnórsson et al. 1983; Arnórsson 1985; Arnórsson and Gunnlaugsson 1985). In other terms, these mineral assemblages constrain f_{CO_2}, at any specified temperature, as described by the following univariant reactions:

$$KAl_3Si_3O_{10}(OH)_2 + 4SiO_2 + CaCO_3 + 3H_2O = KAlSi_3O_8$$
$$+ CaAl_2Si_4O_{12} \cdot 4H_2O + CO_{2(g)} \tag{8.11}$$

$$0.75KAl_3Si_3O_{10}(OH)_2 + 1.5SiO_2 + CaCO_3 = 0.75KAlSi_3O_8$$
$$+ 0.5Ca_2Al_3Si_3O_{12}(OH) + CO_{2(g)} + 0.5H_2O \tag{8.12}$$

$$0.5KAl_3Si_3O_{10}(OH)_2 + 1.5SiO_2 + CaCO_3 = 0.5KAlSi_3O_8$$
$$+ 0.5Ca_2Al_2Si_3O_{10}(OH)_2 + CO_{2(g)} \tag{8.13}$$

$$KAl_3Si_3O_{10}(OH)_2 + 4SiO_2 + CaCO_3 + H_2O = KAlSi_3O_8$$
$$+ CaAl_2Si_4O_{12} \cdot 2H_2O + CO_{2(g)}, \tag{8.14}$$
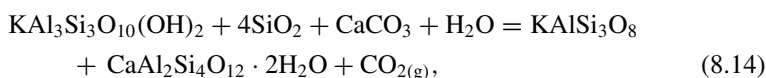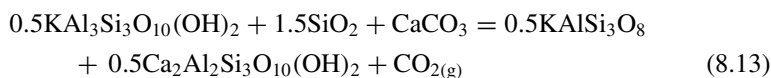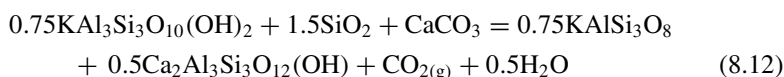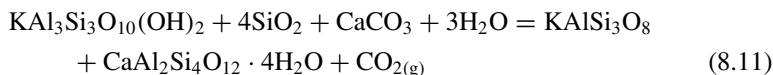
To be noted that reactions (8.11)–(8.14) are obtained by summation of previous reactions. In detail:

- reaction (8.11) is the algebraic sum of either reactions (8.1) and (8.9) or reactions (8.5) and (8.10),
- reaction (8.12) is the algebraic sum of either reactions (8.2) and (8.9) or reactions (8.6) and (8.10),
- reaction (8.13) is the algebraic sum of either reactions (8.3) and (8.9) or reactions (8.7) and (8.10),
- reaction (8.14) is the algebraic sum of either reactions (8.4) and (8.9) or reactions (8.8) and (8.10).

The f_{CO_2}-temperature relationships corresponding to reactions (8.11)–(8.14) define the upper f_{CO_2} value of Ca–Al-silicate stability. At any given temperature, Ca–Al-silicates are stable at lower f_{CO_2} values, whereas calcite is stable at higher f_{CO_2} values. Moreover, the mineral assemblages involved in reactions (8.11)–(8.14) represent the more or less hypothetical condition of full mineral-solution equilibrium. However, none of these CO_2 buffers is ubiquitously efficacious in natural geothermal systems (Grant 1982; Giggenbach 1982). The probable reason for this is that a continuous flux of CO_2 occurs through the geothermal systems in the same manner as the heat flux, as suggested both by field evidence (Mahon et al. 1980) and by water/rock hydrothermal experiments (Kacandes and Grandstaff 1989). Thus, the

univariant equilibrium conditions involving the minerals acting as CO_2 buffers may be established only in some parts of the geothermal systems, whereas in general the f_{CO_2} is an externally fixed parameter. If f_{CO_2} is externally controlled, one of the minerals participating in the univariant reactions (8.11)–(8.14) is no longer part of the equilibrium assemblage, and CO_2 is involved in bivariant reactions, such as reactions (8.9) and (8.10).

8.2 The Activities of Ca-Endmembers in Hydrothermal Ca–Al-Silicates and Calcite

Before gaining further insights from the reactions presented in the previous section, it is useful to recall the available information on the activity of Ca-endmembers in Ca–Al-silicates and calcite from active geothermal systems (Table 8.1), which was discussed in Sects. 4.5.3 for clinozoisite, 4.6.2 for prehnite, 4.7.4 for wairakite, 4.7.5 for laumontite, and 4.9.1 for calcite.

Since adularia, albite and silica minerals occur as pure or relatively pure solid phases in geothermal systems, their activities do not depart significantly from unity, as already noted many times. The same holds true for calcite and, even if to a lesser extent, for laumontite, whereas the activities of wairakite and especially of prehnite and clinozoisite exhibit higher deviations from one, but still relatively limited considering the mean and median values (Table 8.1). The activity of muscovite diverges even more from unity compared to prehnite and clinozoisite. In fact, it varies between 0.007 and 0.875, with an average of 0.654, a median of 0.688 and a standard deviation of 0.156, in 75 white micas from several geothermal systems (see Sect. 4.3.2 for further details).

Table 8.1 Main statistical parameters for the activity of the Ca-endmembers in Ca–Al-silicates and calcite from active geothermal systems

Ca-endmember	Solid solution	N	Mean	Median	Std dev	Min	Max
Clinozoisite	Clinozoisite/epidote	436	0.703	0.706	0.057	0.523	0.888
Prehnite	Prehnite/ferri-prehnite	127	0.763	0.779	0.154	0.373	0.998
Wairakite	Wairakite/analcime	136	0.891	0.920	0.090	0.573	0.999
Laumontite	Laumontite/alkali-laumontite	45	0.946	0.951	0.031	0.873	0.992
Calcite	Calcite-rich trigonal carbonate	313	0.972	0.988	0.043	0.705	1.000

8.3 The Log K of the K–Ca and Na–Ca Exchange Reactions and of the Univariant Reactions Involving Calcite and a Ca–Al-Silicate

Assuming that the activity of water does not differ significantly from 1, if the ionic strength of the aqueous phase is less than ~1 mol/kg, the decimal logarithm of the thermodynamic equilibrium constants of the reactions presented in Sect. 8.1 can be generally written in the following simplified forms:

$$\log K_{K-Ca,Lmt} \cong \log\left(\frac{a_{K^+}^2}{a_{Ca^{2+}}}\right) + \log a_{Lmt} \tag{8.15}$$

$$\log K_{K-Ca,Czo} \cong \log\left(\frac{a_{K^+}^2}{a_{Ca^{2+}}}\right) + 0.25 \cdot \log a_{Ms} + 0.5 \cdot \log a_{Czo} \tag{8.16}$$

$$\log K_{K-Ca,Prh} \cong \log\left(\frac{a_{K^+}^2}{a_{Ca^{2+}}}\right) + 0.5 \cdot \log a_{Ms} + 0.5 \cdot \log a_{Prh} \tag{8.17}$$

$$\log K_{K-Ca,Wrk} \cong \log\left(\frac{a_{K^+}^2}{a_{Ca^{2+}}}\right) + \log a_{Wrk} \tag{8.18}$$

$$\log K_{Na-Ca,Lmt} \cong \log\left(\frac{a_{Na^+}^2}{a_{Ca^{2+}}}\right) + \log a_{Lmt} \tag{8.19}$$

$$\log K_{Na-Ca,Czo} \cong \log\left(\frac{a_{Na^+}^2}{a_{Ca^{2+}}}\right) + 0.25 \cdot \log a_{Ms} + 0.5 \cdot \log a_{Czo} \tag{8.20}$$

$$\log K_{Na-Ca,Prh} \cong \log\left(\frac{a_{Na^+}^2}{a_{Ca^{2+}}}\right) + 0.5 \cdot \log a_{Ms} + 0.5 \cdot \log a_{Prh} \tag{8.21}$$

$$\log K_{Na-Ca,Wrk} \cong \log\left(\frac{a_{Na^+}^2}{a_{Ca^{2+}}}\right) + \log a_{Wrk} \tag{8.22}$$

$$\log K_{K-Ca,Cal} \cong \log\left(\frac{a_{K^+}^2}{a_{Ca^{2+}}}\right) - \log f_{CO_2} + \log a_{Ms} \tag{8.23}$$

$$\log K_{Na-Ca,Cal} \cong \log\left(\frac{a_{Na^+}^2}{a_{Ca^{2+}}}\right) - \log f_{CO_2} + \log a_{Ms} \tag{8.24}$$

$$\log K_{Lmt-Cal} \cong \log f_{CO_2} + \log a_{Lmt} - \log a_{Ms} \tag{8.25}$$

$$\log K_{Czo-Cal} \cong \log f_{CO_2} + 0.5 \cdot \log a_{Czo} - 0.75 \cdot \log a_{Ms} \qquad (8.26)$$

$$\log K_{Prh-Cal} \cong \log f_{CO_2} + 0.5 \cdot \log a_{Prh} - 0.5 \cdot \log a_{Ms} \qquad (8.27)$$

$$\log K_{Wrk-Cal} \cong \log f_{CO_2} + \log a_{Wrk} - \log a_{Ms} \qquad (8.28)$$

As discussed in Sects. 4.2.3 and 5.3.3, Al–Si order-disorder on the tetrahedral sites of adularia causes further complications. Therefore, adopting the same approach of Sects. 6.1 and 7.1, adularias with ordering parameter Z varying from 0 (i.e., high-sanidine) to 1 (i.e., maximum-microcline) at steps of 0.1 units were alternatively considered to take part to reactions (8.1)–(8.4), (8.6), (8.7), and (8.9)–(8.14). The silica mineral involved in these reactions was assumed to be chalcedony at T < 175 °C or quartz/chalcedony at T > 175 °C. The thermodynamic properties of these reactions were computed as a function of temperature, at pressure of 1 bar for T < 100 °C and at water saturation pressure for T ≥ 100 °C, using the SUPCRT92 code.

8.4 Derivation of the Activity-Based Theoretical K–Ca and Na–Ca Geothermometers and f_{CO_2}-Indicators

The logarithm of the thermodynamic equilibrium constants of reactions (8.1)–(8.10) for pure solid phases were fitted against both the inverse of the absolute temperature and the ordering parameter of adularia (if present in the reaction), considering as two distinct datasets the data below 175 °C, with chalcedony controlling undissociated SiO_2, and those above 175 °C, with quartz/chalcedony governing undissociated SiO_2. Each regression equation and the average activities of pertinent solid phases were then inserted into the corresponding relation linking the log K to the K^2/Ca- and Na^2/Ca-log activity ratios, i.e., Eqs. (8.15)–(8.24).

The relations derived from Eqs. (8.15) to (8.22) were solved with respect to temperature, thus obtaining four K–Ca geothermometers and four Na–Ca geothermometers. The relationships resulting from Eqs. (8.23) and (8.24) were solved with respect to the logarithm of CO_2 fugacity, thus obtaining a K–Ca f_{CO_2}-indicator and a Na–Ca f_{CO_2}-indicator.

The uncertainties caused by variations in the activities of relevant components in the solid solutions of interest, that is muscovite in illite, laumontite in laumontite/alkali-laumontite, clinozoisite in clinozoisite/epidote, prehnite in prehnite/ferri-prehnite, and wairakite in wairakite/analcime were evaluated considering the average activities plus one standard deviation and the average activities minus one standard deviation (see below).

8.4.1 The Theoretical K–Ca and Na–Ca Laumontite Geothermometers

For reactions (8.1) and (8.5), comprising laumontite, the following four geothermometric equations were obtained from Eqs. (8.15) and (8.19) and the log $K_{K–Ca,Lmt}$ and log $K_{Na–Ca,Lmt}$ values listed in Tables 8.2 and 8.3, respectively:

$$T_{K-Ca,Lmt} \,(°C) = \frac{2481.5 + 1158.1 \cdot Z}{4.0237 + 1.4861 \cdot Z - \log\left(\frac{a_{K^+}^2}{a_{Ca^{2+}}}\right)} - 273.15, \quad \text{for T} < 175\,°C \tag{8.29}$$

$$T_{K-Ca,Lmt} \,(°C) = \frac{2100.3 + 1157.4 \cdot Z}{3.3178 + 1.4845 \cdot Z - \log\left(\frac{a_{K^+}^2}{a_{Ca^{2+}}}\right)} - 273.15,$$
$$\text{for } 175 < T < 325\,°C \tag{8.30}$$

$$T_{Na-Ca,Lmt} \,(°C) = \frac{940.13}{2.4914 - \log\left(\frac{a_{Na^+}^2}{a_{Ca^{2+}}}\right)} - 273.15, \quad \text{for T} < 175\,°C \tag{8.31}$$

$$T_{Na-Ca,Lmt} \,(°C) = \frac{1050.2}{2.9090 - \log\left(\frac{a_{Na^+}^2}{a_{Ca^{2+}}}\right)} - 273.15, \quad \text{for } 175 < T < 325\,°C \tag{8.32}$$

It must be noted that the log K values of reaction (8.5), which are reported in Table 8.3, depend on temperature only because adularia is not involved in this reaction. The average value of log a_{Lmt}, -0.0241, is considered in Eqs. (8.29)–(8.32). Due to deviations of laumontite activity of $+1\sigma$ and -1σ from the mean value, log a_{Lmt} assumes the values -0.0101 and -0.0386, respectively. These variations in log a_{Lmt}, determine differences of ±0.3 to $\pm1.1\,°C$, ±0.9 to $\pm1.8\,°C$, ±1.1 to $\pm3.0\,°C$, and ±2.7 to $\pm5.0\,°C$ in the temperatures calculated by means of Eqs. (8.29), (8.30), (8.31), and (8.32), respectively, representing their nominal errors.

8.4.2 The Theoretical K–Ca and Na–Ca Clinozoisite Geothermometers

For reactions (8.2) and (8.6), involving clinozoisite, the following four geothermometric functions were obtained, based on Eqs. (8.16) and (8.20) and the log $K_{K–Ca,Czo}$ and log $K_{Na–Ca,Czo}$ values reported in Tables 8.4 and 8.5, respectively:

Table 8.2 Logarithm of the thermodynamic equilibrium constant of reaction (8.1), log $K_{K–Ca,Lmt}$, for pure laumontite, chalcedony (for T < 175 °C) or quartz/chalcedony (for T > 175 °C), and adularia, as a function of the temperature and the ordering parameter Z of adularia (P = 1 bar for T < 100 °C; P = P_{sat} for T ≥ 100 °C)

T (°C)	Z = 1	Z = 0.9	Z = 0.8	Z = 0.7	Z = 0.6	Z = 0.5	Z = 0.4	Z = 0.3	Z = 0.2	Z = 0.1	Z = 0
0.01	−7.9665	−7.6912	−7.4158	−7.1404	−6.8650	−6.5897	−6.3143	−6.0389	−5.7635	−5.4882	−5.2128
25	−6.7611	−6.5213	−6.2815	−6.0416	−5.8018	−5.5619	−5.3221	−5.0823	−4.8424	−4.6026	−4.3627
50	−5.7679	−5.5581	−5.3483	−5.1386	−4.9288	−4.7190	−4.5092	−4.2994	−4.0896	−3.8798	−3.6700
75	−4.9389	−4.7548	−4.5708	−4.3867	−4.2027	−4.0186	−3.8346	−3.6505	−3.4665	−3.2824	−3.0984
100	−4.2385	−4.0768	−3.9150	−3.7532	−3.5915	−3.4297	−3.2680	−3.1062	−2.9444	−2.7827	−2.6209
125	−3.6403	−3.4980	−3.3557	−3.2135	−3.0712	−2.9289	−2.7866	−2.6444	−2.5021	−2.3598	−2.2175
150	−3.1238	−2.9987	−2.8736	−2.7485	−2.6235	−2.4984	−2.3733	−2.2482	−2.1231	−1.9980	−1.8729
175	−2.6734	−2.5635	−2.4537	−2.3439	−2.2341	−2.1242	−2.0144	−1.9046	−1.7948	−1.6849	−1.5751
175	−2.4930	−2.3831	−2.2733	−2.1635	−2.0536	−1.9438	−1.8340	−1.7242	−1.6143	−1.5045	−1.3947
200	−2.1058	−2.0096	−1.9134	−1.8173	−1.7211	−1.6249	−1.5287	−1.4326	−1.3364	−1.2402	−1.1441
225	−1.7611	−1.6771	−1.5932	−1.5093	−1.4254	−1.3416	−1.2577	−1.1738	−1.0899	−1.0060	−0.9221
250	−1.4495	−1.3767	−1.3039	−1.2311	−1.1583	−1.0855	−1.0127	−0.9400	−0.8672	−0.7944	−0.7216
275	−1.1640	−1.1012	−1.0385	−0.9758	−0.9131	−0.8504	−0.7877	−0.7250	−0.6623	−0.5996	−0.5369
300	−0.9023	−0.8486	−0.7951	−0.7416	−0.6882	−0.6347	−0.5812	−0.5277	−0.4742	−0.4207	−0.3673
325	−0.6723	−0.6270	−0.5820	−0.5369	−0.4919	−0.4469	−0.4018	−0.3568	−0.3117	−0.2667	−0.2217
350	−0.5027	−0.4650	−0.4278	−0.3905	−0.3532	−0.3159	−0.2786	−0.2413	−0.2041	−0.1668	−0.1295

Table 8.3 Logarithm of the thermodynamic equilibrium constant of reaction (8.5), log $K_{Na–Ca,Lmt}$, for pure laumontite, chalcedony (for T < 175 °C) or quartz/chalcedony (for T > 175 °C), and albite, as a function of temperature (P = 1 bar for T < 100 °C; P = P_{sat} for T ≥ 100 °C)

T (°C)	0.01	25	50	75	100	125	150	175
log K	−0.9783	−0.6816	−0.4386	−0.2330	−0.0548	0.1025	0.2440	0.3731
T (°C)	175	200	225	250	275	300	325	350
log K	0.5535	0.6634	0.7672	0.8671	0.9647	1.0581	1.1375	1.1749

$$T_{K–Ca,Czo}\,(°C) = \frac{1302.9 \cdot Z + 3697.9}{6.3540 + 1.6719 \cdot Z - \log\left(\frac{a_{K^+}^2}{a_{Ca^{2+}}}\right)} - 273.15, \quad \text{for } T < 175\,°C \tag{8.33}$$

$$T_{K–Ca,Czo}\,(°C) = \frac{1302.1 \cdot Z + 4121.3}{7.6909 + 1.6700 \cdot Z - \log\left(\frac{a_{K^+}^2}{a_{Ca^{2+}}}\right)} - 273.15,$$
$$\text{for } 175 < T < 325\,°C \tag{8.34}$$

$$T_{Na–Ca,Czo}\,(°C) = \frac{144.81 \cdot Z + 2170.4}{4.8576 + 0.1859 \cdot Z - \log\left(\frac{a_{Na^+}^2}{a_{Ca^{2+}}}\right)} - 273.15, \quad \text{for } T < 175\,°C \tag{8.35}$$

$$T_{Na–Ca,Czo}\,(°C) = \frac{144.72 \cdot Z + 3042.6}{7.2239 + 0.1856 \cdot Z - \log\left(\frac{a_{Na^+}^2}{a_{Ca^{2+}}}\right)} - 273.15,$$
$$\text{for } 175 < T < 325\,°C \tag{8.36}$$

The average value of the term $0.25 \cdot \log a_{Ms} + 0.5 \cdot \log a_{Czo}$, -0.1227, is considered in Eqs. (8.33)–(8.36). Due to deviations of clinozoisite and muscovite activity of $+1\sigma$ and -1σ from the mean values, the term $0.25 \cdot \log a_{Ms} + 0.5 \cdot \log a_{Czo}$ assumes the values -0.0825 and -0.1706, respectively. These variations in the term $0.25 \cdot \log a_{Ms} + 0.5 \cdot \log a_{Czo}$, cause differences of ± 0.7 to ± 2.3 °C, ± 1.8 to ± 3.8 °C, ± 1.3 to ± 4.1 °C, and ± 2.5 to ± 5.3 °C in the temperatures computed by means of Eqs. (8.33), (8.34), (8.35), and (8.36), respectively, representing their nominal uncertainties.

8.4.3 The Theoretical K–Ca and Na–Ca Prehnite Geothermometers

For reactions (8.3) and (8.7), including prehnite, the following four geothermometric equations were obtained on the basis of Eqs. (8.17) and (8.21) and the log $K_{K–Ca,Prh}$ and log $K_{Na–Ca,Prh}$ values listed in Tables 8.6 and 8.7, respectively:

Table 8.4 Logarithm of the thermodynamic equilibrium constant of reaction (8.2), log $K_{K-Ca,Czo}$, for pure clinozoisite, muscovite, chalcedony (for T < 175 °C) or quartz/chalcedony (for T > 175 °C), and adularia, as a function of the temperature and the ordering parameter Z of adularia (P = 1 bar for T < 100 °C; P = P_{sat} for T ≥ 100 °C)

T (°C)	Z = 1	Z = 0.9	Z = 0.8	Z = 0.7	Z = 0.6	Z = 0.5	Z = 0.4	Z = 0.3	Z = 0.2	Z = 0.1	Z = 0
0.01	−10.3855	−10.0757	−9.7659	−9.4561	−9.1463	−8.8365	−8.5267	−8.2169	−7.9071	−7.5973	−7.2875
25	−8.8680	−8.5982	−8.3284	−8.0585	−7.7887	−7.5189	−7.2491	−6.9793	−6.7094	−6.4396	−6.1698
50	−7.5821	−7.3461	−7.1101	−6.8741	−6.6381	−6.4021	−6.1661	−5.9300	−5.6940	−5.4580	−5.2220
75	−6.4769	−6.2699	−6.0628	−5.8557	−5.6487	−5.4416	−5.2346	−5.0275	−4.8205	−4.6134	−4.4063
100	−5.5145	−5.3325	−5.1505	−4.9685	−4.7866	−4.6046	−4.4226	−4.2406	−4.0586	−3.8766	−3.6946
125	−4.6662	−4.5061	−4.3460	−4.1860	−4.0259	−3.8659	−3.7058	−3.5457	−3.3857	−3.2256	−3.0656
150	−3.9100	−3.7693	−3.6286	−3.4878	−3.3471	−3.2064	−3.0656	−2.9249	−2.7842	−2.6435	−2.5027
175	−3.2289	−3.1053	−2.9818	−2.8582	−2.7347	−2.6111	−2.4876	−2.3640	−2.2405	−2.1169	−1.9934
175	−2.8229	−2.6994	−2.5758	−2.4523	−2.3287	−2.2052	−2.0816	−1.9581	−1.8345	−1.7110	−1.5874
200	−2.2249	−2.1167	−2.0085	−1.9003	−1.7921	−1.6839	−1.5757	−1.4675	−1.3593	−1.2511	−1.1429
225	−1.6748	−1.5804	−1.4860	−1.3916	−1.2973	−1.2029	−1.1085	−1.0141	−0.9198	−0.8254	−0.7310
250	−1.1627	−1.0807	−0.9988	−0.9169	−0.8350	−0.7532	−0.6713	−0.5894	−0.5075	−0.4256	−0.3438
275	−0.6804	−0.6097	−0.5392	−0.4687	−0.3982	−0.3276	−0.2571	−0.1866	−0.1160	−0.0455	0.0250
300	−0.2251	−0.1647	−0.1045	−0.0444	0.0158	0.0760	0.1361	0.1963	0.2565	0.3166	0.3768
325	0.1963	0.2473	0.2979	0.3486	0.3993	0.4499	0.5006	0.5513	0.6020	0.6526	0.7033
350	0.5562	0.5985	0.6405	0.6824	0.7243	0.7663	0.8082	0.8502	0.8921	0.9341	0.9760

Table 8.5 Logarithm of the thermodynamic equilibrium constant of reaction (8.6), log $K_{Na–Ca,Cz0}$, for pure clinozoisite, muscovite, chalcedony (for T < 175 °C) or quartz/chalcedony (for T > 175 °C), adularia, and albite, as a function of the temperature and the ordering parameter Z of adularia (P = 1 bar for T < 100 °C; P = P_{sat} for T ≥ 100 °C)

T (°C)	Z = 1	Z = 0.9	Z = 0.8	Z = 0.7	Z = 0.6	Z = 0.5	Z = 0.4	Z = 0.3	Z = 0.2	Z = 0.1	Z = 0
0.01	−3.3972	−3.3628	−3.3284	−3.2940	−3.2595	−3.2251	−3.1907	−3.1563	−3.1219	−3.0874	−3.0530
25	−2.7884	−2.7585	−2.7285	−2.6985	−2.6685	−2.6385	−2.6086	−2.5786	−2.5486	−2.5186	−2.4886
50	−2.2528	−2.2266	−2.2004	−2.1741	−2.1479	−2.1217	−2.0955	−2.0692	−2.0430	−2.0168	−1.9906
75	−1.7710	−1.7480	−1.7250	−1.7020	−1.6790	−1.6560	−1.6330	−1.6100	−1.5869	−1.5639	−1.5409
100	−1.3308	−1.3106	−1.2903	−1.2701	−1.2499	−1.2297	−1.2095	−1.1892	−1.1690	−1.1488	−1.1286
125	−0.9233	−0.9055	−0.8878	−0.8700	−0.8522	−0.8344	−0.8166	−0.7988	−0.7811	−0.7633	−0.7455
150	−0.5422	−0.5266	−0.5109	−0.4953	−0.4797	−0.4640	−0.4484	−0.4328	−0.4171	−0.4015	−0.3859
175	−0.1825	−0.1687	−0.1550	−0.1413	−0.1275	−0.1138	−0.1001	−0.0864	−0.0726	−0.0589	−0.0452
175	0.2235	0.2372	0.2510	0.2647	0.2784	0.2922	0.3059	0.3196	0.3333	0.3471	0.3608
200	0.5443	0.5564	0.5684	0.5804	0.5924	0.6045	0.6165	0.6285	0.6405	0.6525	0.6646
225	0.8534	0.8639	0.8744	0.8849	0.8954	0.9058	0.9163	0.9268	0.9373	0.9478	0.9583
250	1.1539	1.1630	1.1721	1.1812	1.1903	1.1994	1.2085	1.2176	1.2267	1.2358	1.2449
275	1.4483	1.4561	1.4640	1.4718	1.4796	1.4875	1.4953	1.5031	1.5110	1.5188	1.5266
300	1.7353	1.7420	1.7487	1.7554	1.7621	1.7688	1.7754	1.7821	1.7888	1.7955	1.8022
325	2.0061	2.0118	2.0174	2.0231	2.0287	2.0343	2.0400	2.0456	2.0512	2.0568	2.0625
350	2.2337	2.2384	2.2431	2.2477	2.2524	2.2571	2.2617	2.2664	2.2710	2.2757	2.2804

Table 8.6 Logarithm of the thermodynamic equilibrium constant of reaction (8.3), log $K_{K-Ca,Prh}$, for pure prehnite, muscovite, chalcedony (for T < 175 °C) or quartz/chalcedony (for T > 175 °C), and adularia, as a function of the temperature and the ordering parameter Z of adularia (P = 1 bar for T < 100 °C; P = P_{sat} for T ≥ 100 °C)

T (°C)	Z = 1	Z = 0.9	Z = 0.8	Z = 0.7	Z = 0.6	Z = 0.5	Z = 0.4	Z = 0.3	Z = 0.2	Z = 0.1	Z = 0
0.01	−8.3997	−8.0555	−7.7113	−7.3671	−7.0228	−6.6786	−6.3344	−5.9902	−5.6459	−5.3017	−4.9575
25	−7.1701	−6.8703	−6.5705	−6.2707	−5.9709	−5.6711	−5.3713	−5.0715	−4.7717	−4.4719	−4.1721
50	−6.1320	−5.8697	−5.6075	−5.3452	−5.0830	−4.8208	−4.5585	−4.2963	−4.0341	−3.7718	−3.5096
75	−5.2427	−5.0126	−4.7825	−4.5525	−4.3224	−4.0924	−3.8623	−3.6322	−3.4022	−3.1721	−2.9420
100	−4.4705	−4.2683	−4.0661	−3.8639	−3.6617	−3.4595	−3.2573	−3.0551	−2.8529	−2.6507	−2.4485
125	−3.7914	−3.6136	−3.4357	−3.2579	−3.0800	−2.9022	−2.7243	−2.5465	−2.3686	−2.1908	−2.0130
150	−3.1870	−3.0306	−2.8742	−2.7179	−2.5615	−2.4052	−2.2488	−2.0924	−1.9361	−1.7797	−1.6233
175	−2.6429	−2.5056	−2.3683	−2.2310	−2.0938	−1.9565	−1.8192	−1.6819	−1.5446	−1.4074	−1.2701
175	−2.2369	−2.0996	−1.9623	−1.8251	−1.6878	−1.5505	−1.4132	−1.2759	−1.1387	−1.0014	−0.8641
200	−1.7634	−1.6431	−1.5229	−1.4027	−1.2825	−1.1623	−1.0420	−0.9218	−0.8016	−0.6814	−0.5612
225	−1.3271	−1.2221	−1.1172	−1.0124	−0.9075	−0.8027	−0.6978	−0.5929	−0.4881	−0.3832	−0.2784
250	−0.9194	−0.8283	−0.7373	−0.6463	−0.5554	−0.4644	−0.3734	−0.2824	−0.1914	−0.1005	−0.0095
275	−0.5336	−0.4550	−0.3767	−0.2983	−0.2200	−0.1416	−0.0632	0.0151	0.0935	0.1719	0.2502
300	−0.1677	−0.1006	−0.0337	0.0331	0.1000	0.1668	0.2337	0.3005	0.3674	0.4342	0.5011
325	0.1704	0.2270	0.2833	0.3396	0.3959	0.4522	0.5085	0.5648	0.6211	0.6774	0.7337
350	0.4523	0.4993	0.5459	0.5925	0.6391	0.6857	0.7323	0.7789	0.8255	0.8722	0.9188

Table 8.7 Logarithm of the thermodynamic equilibrium constant of reaction (8.7), log $K_{Na-Ca,Prh}$, for pure prehnite, muscovite, chalcedony (for T < 175 °C) or quartz/chalcedony (for T > 175 °C), adularia, and albite, as a function of the temperature and the ordering parameter Z of adularia (P = 1 bar for T < 100 °C; P = P_{sat} for T ≥ 100 °C)

T (°C)	Z = 1	Z = 0.9	Z = 0.8	Z = 0.7	Z = 0.6	Z = 0.5	Z = 0.4	Z = 0.3	Z = 0.2	Z = 0.1	Z = 0
0.01	−1.4115	−1.3426	−1.2738	−1.2049	−1.1361	−1.0672	−0.9984	−0.9295	−0.8607	−0.7919	−0.7230
25	−1.0905	−1.0305	−0.9706	−0.9106	−0.8507	−0.7907	−0.7307	−0.6708	−0.6108	−0.5509	−0.4909
50	−0.8026	−0.7502	−0.6977	−0.6453	−0.5928	−0.5404	−0.4879	−0.4355	−0.3831	−0.3306	−0.2782
75	−0.5368	−0.4907	−0.4447	−0.3987	−0.3527	−0.3067	−0.2607	−0.2147	−0.1687	−0.1226	−0.0766
100	−0.2868	−0.2464	−0.2059	−0.1655	−0.1250	−0.0846	−0.0442	−0.0037	0.0367	0.0772	0.1176
125	−0.0486	−0.0130	0.0226	0.0581	0.0937	0.1293	0.1648	0.2004	0.2360	0.2716	0.3071
150	0.1808	0.2121	0.2434	0.2746	0.3059	0.3372	0.3684	0.3997	0.4310	0.4623	0.4935
175	0.4036	0.4310	0.4585	0.4859	0.5134	0.5409	0.5683	0.5958	0.6232	0.6507	0.6781
175	0.8095	0.8370	0.8645	0.8919	0.9194	0.9468	0.9743	1.0017	1.0292	1.0567	1.0841
200	1.0059	1.0299	1.0540	1.0780	1.1021	1.1261	1.1501	1.1742	1.1982	1.2223	1.2463
225	1.2012	1.2222	1.2431	1.2641	1.2851	1.3061	1.3270	1.3480	1.3690	1.3899	1.4109
250	1.3972	1.4154	1.4336	1.4518	1.4700	1.4882	1.5064	1.5246	1.5428	1.5610	1.5792
275	1.5951	1.6108	1.6265	1.6422	1.6578	1.6735	1.6892	1.7048	1.7205	1.7362	1.7519
300	1.7927	1.8061	1.8195	1.8329	1.8462	1.8596	1.8730	1.8863	1.8997	1.9131	1.9265
325	1.9802	1.9915	2.0028	2.0141	2.0253	2.0366	2.0479	2.0591	2.0704	2.0816	2.0929
350	2.1298	2.1392	2.1485	2.1579	2.1672	2.1765	2.1858	2.1952	2.2045	2.2138	2.2231

$$T_{\text{K}-\text{Ca,Prh}} \, (^{\circ}\text{C}) = \frac{1447.7 \cdot Z + 2573.9}{4.6093 + 1.8577 \cdot Z - \log\left(\frac{a_{\text{K}^+}^2}{a_{\text{Ca}^{2+}}}\right)} - 273.15, \quad \text{for T} < 175\,^{\circ}\text{C}$$

(8.37)

$$T_{\text{K}-\text{Ca,Prh}} \, (^{\circ}\text{C}) = \frac{1446.7 \cdot Z + 2876.0}{5.6691 + 1.8555 \cdot Z - \log\left(\frac{a_{\text{K}^+}^2}{a_{\text{Ca}^{2+}}}\right)} - 273.15,$$

$$\text{for } 175 < \text{T} < 325\,^{\circ}\text{C}$$

(8.38)

$$T_{\text{Na}-\text{Ca,Prh}} \, (^{\circ}\text{C}) = \frac{289.51 \cdot Z + 1035.4}{3.0844 + 0.3715 \cdot Z - \log\left(\frac{a_{\text{Na}^+}^2}{a_{\text{Ca}^{2+}}}\right)} - 273.15, \quad \text{for T} < 175\,^{\circ}\text{C}$$

(8.39)

$$T_{\text{Na}-\text{Ca,Prh}} \, (^{\circ}\text{C}) = \frac{289.33 \cdot Z + 1804.7}{5.3085 + 0.3711 \cdot Z - \log\left(\frac{a_{\text{Na}^+}^2}{a_{\text{Ca}^{2+}}}\right)} - 273.15,$$

$$\text{for } 175 < \text{T} < 325\,^{\circ}\text{C}$$

(8.40)

The mean value of the term $0.50 \cdot \log a_{\text{Ms}} + 0.5 \cdot \log a_{\text{Prh}}$, -0.1509, is considered in Eqs. (8.37)–(8.40). Owing to departures of prehnite and muscovite activity of $+1\sigma$ and -1σ from the mean values, the term $0.50 \cdot \log a_{\text{Ms}} + 0.5 \cdot \log a_{\text{Prh}}$ becomes equal to -0.0646 and -0.2591, respectively. These changes in the term $0.50 \cdot \log a_{\text{Ms}} + 0.5 \cdot \log a_{\text{Prh}}$, determine differences of ± 1.6 to ± 5.3 °C, ± 4.0 to ± 9.6 °C, ± 4.5 to ± 14.4 °C, and ± 8.4 to ± 17.9 °C in the temperatures computed by means of Eqs. (8.37), (8.38), (8.39), and (8.40), respectively, representing their nominal errors.

8.4.4   The Theoretical K–Ca and Na–Ca Wairakite Geothermometers

For reactions (8.4) and (8.8), involving wairakite, the following four geothermometric functions were obtained based on Eqs. (8.18) and (8.22) and the log $K_{\text{K}-\text{Ca,Wrk}}$ and log $K_{\text{Na}-\text{Ca,Wrk}}$ values reported in Tables 8.8 and 8.9, respectively:

$$T_{\text{K}-\text{Ca,Wrk}} \, (^{\circ}\text{C}) = \frac{1158.2 \cdot Z + 5457.0}{9.5776 + 1.4861 \cdot Z - \log\left(\frac{a_{\text{K}^+}^2}{a_{\text{Ca}^{2+}}}\right)} - 273.15, \quad \text{for T} < 175\,^{\circ}\text{C}$$

(8.41)

$$T_{\text{K}-\text{Ca,Wrk}} \, (^{\circ}\text{C}) = \frac{1157.4 \cdot Z + 5520.6}{9.8775 + 1.4844 \cdot Z - \log\left(\frac{a_{\text{K}^+}^2}{a_{\text{Ca}^{2+}}}\right)} - 273.15,$$

$$\text{for } 175 < \text{T} < 325\,^{\circ}\text{C}$$

(8.42)

Table 8.8 Logarithm of the thermodynamic equilibrium constant of reaction (8.4), log $K_{K-Ca,Wrk}$, for pure wairakite, chalcedony (for $T < 175$ °C) or quartz/chalcedony (for $T > 175$ °C), and adularia, as a function of the temperature and the ordering parameter Z of adularia ($P = 1$ bar for $T < 100$ °C; $P = P_{sat}$ for $T \geq 100$ °C)

T (°C)	Z = 1	Z = 0.9	Z = 0.8	Z = 0.7	Z = 0.6	Z = 0.5	Z = 0.4	Z = 0.3	Z = 0.2	Z = 0.1	Z = 0
0.01	−13.2163	−12.9410	−12.6656	−12.3902	−12.1148	−11.8394	−11.5641	−11.2887	−11.0133	−10.7379	−10.4626
25	−11.1706	−10.9308	−10.6909	−10.4511	−10.2112	−9.9714	−9.7316	−9.4917	−9.2519	−9.0120	−8.7722
50	−9.4480	−9.2382	−9.0284	−8.8186	−8.6088	−8.3991	−8.1893	−7.9795	−7.7697	−7.5599	−7.3501
75	−7.9783	−7.7942	−7.6101	−7.4261	−7.2420	−7.0580	−6.8739	−6.6899	−6.5058	−6.3218	−6.1377
100	−6.7091	−6.5473	−6.3855	−6.2238	−6.0620	−5.9002	−5.7385	−5.5767	−5.4149	−5.2532	−5.0914
125	−5.6013	−5.4590	−5.3167	−5.1744	−5.0322	−4.8899	−4.7476	−4.6053	−4.4631	−4.3208	−4.1785
150	−4.6245	−4.4994	−4.3743	−4.2492	−4.1241	−3.9990	−3.8739	−3.7488	−3.6238	−3.4987	−3.3736
175	−3.7552	−3.6454	−3.5356	−3.4257	−3.3159	−3.2061	−3.0963	−2.9864	−2.8766	−2.7668	−2.6570
175	−3.5748	−3.4649	−3.3551	−3.2453	−3.1355	−3.0256	−2.9158	−2.8060	−2.6962	−2.5863	−2.4765
200	−2.8041	−2.7079	−2.6117	−2.5155	−2.4194	−2.3232	−2.2270	−2.1309	−2.0347	−1.9385	−1.8424
225	−2.1061	−2.0221	−1.9382	−1.8544	−1.7705	−1.6866	−1.6027	−1.5188	−1.4349	−1.3510	−1.2671
250	−1.4674	−1.3945	−1.3218	−1.2490	−1.1762	−1.1034	−1.0306	−0.9579	−0.8851	−0.8123	−0.7395
275	−0.8775	−0.8146	−0.7520	−0.6893	−0.6266	−0.5639	−0.5012	−0.4385	−0.3758	−0.3131	−0.2504
300	−0.3312	−0.2775	−0.2240	−0.1705	−0.1171	−0.0636	−0.0101	0.0434	0.0969	0.1503	0.2038
325	0.1660	0.2113	0.2563	0.3014	0.3464	0.3915	0.4365	0.4816	0.5266	0.5716	0.6167
350	0.5877	0.6253	0.6626	0.6999	0.7372	0.7745	0.8118	0.8490	0.8863	0.9236	0.9609

Table 8.9   Logarithm of the thermodynamic equilibrium constant of reaction (8.8), $\log K_{Na–Ca,Wrk}$, for pure wairakite, chalcedony (for T < 175 °C) or quartz/chalcedony (for T > 175 °C), and albite, as a function of temperature (P = 1 bar for T < 100 °C; P = P_{sat} for T ≥ 100 °C)

T (°C)	0.01	25	50	75	100	125	150	175
log K	−6.2281	−5.0910	−4.1187	−3.2723	−2.5253	−1.8584	−1.2567	−0.7088
T (°C)	175	200	225	250	275	300	325	350
log K	−0.5283	−0.0348	0.4221	0.8492	1.2512	1.6292	1.9758	2.2653

$$T_{Na–Ca,Wrk}\,(°C) = 0.1490 \cdot \chi^3 + 3.9720 \cdot \chi^2 + 52.5016 \cdot \chi + 207.866,$$
$$\text{for } T < 175\,°C \tag{8.43}$$

$$T_{Na–Ca,Wrk}\,(°C) = 0.5157 \cdot \chi^3 + 3.6160 \cdot \chi^2 + 52.5514 \cdot \chi + 199.312,$$
$$\text{for } 175 < T < 325\,°C \tag{8.44}$$

In Eqs. (8.43) and (8.44), $\chi = \log\!\left(a_{Na^+}^2 / a_{Ca^{2+}}\right)$.

To be noted that the log K values of reaction (8.8), which are shown in Table 8.9, are function of temperature only because adularia does not take part to this reaction. The average value of $\log a_{Wrk}$, −0.0501, is considered in Eqs. (8.41)–(8.44). Due to deviations of wairakite activity of +1σ and −1σ from the average value, $\log a_{Wrk}$ assumes the values −0.0083 and −0.0964, respectively. These variations in $\log a_{Wrk}$, determine differences of ±0.5 to ±1.4 °C, ±1.3 to ±2.7 °C, ±0.9 to ±2.2 °C, and ±2.1 to ±3.4 °C in the temperatures calculated by means of Eqs. (8.41), (8.42), (8.43), and (8.44), respectively, representing their nominal uncertainties.

8.4.5   The Theoretical K–Ca and Na–Ca Calcite f_{CO_2}-Indicators

For reactions (8.9) and (8.10), comprising calcite, the following four equations were obtained on the basis of Eqs. (8.23) and (8.24) and the $\log K_{K–Ca,Cal}$ and $\log K_{Na–Ca,Cal}$ values given in Tables 8.10 and 8.11, respectively

$$\log f_{CO_2,K–Ca} = \log\!\left(\frac{a_{K^+}^2}{a_{Ca^{2+}}}\right) + \left(\frac{1737.2}{T} - 2.2291\right) \cdot Z$$
$$- \frac{49,305}{T^2} - \frac{1506.0}{T} + 3.5345 \tag{8.45}$$

$$\log f_{CO_2,K–Ca} = \log\!\left(\frac{a_{K^+}^2}{a_{Ca^{2+}}}\right) + \left(\frac{1736.3}{T} - 2.2270\right) \cdot Z$$

Table 8.10 Logarithm of the thermodynamic equilibrium constant of reaction (8.9), log $K_{K-Ca,Ca}$, for pure calcite, adularia, muscovite, and chalcedony (for T < 175 °C) or quartz/chalcedony (for T > 175 °C), as a function of the temperature and the ordering parameter Z of adularia (P = 1 bar for T < 100 °C; P = P$_{sat}$ for T ≥ 100 °C)

T (°C)	Z = 1	Z = 0.9	Z = 0.8	Z = 0.7	Z = 0.6	Z = 0.5	Z = 0.4	Z = 0.3	Z = 0.2	Z = 0.1	Z = 0
0.01	−1.6797	−1.2667	−0.8536	−0.4405	−0.0275	0.3856	0.7987	1.2117	1.6248	2.0379	2.4509
25	−1.7055	−1.3457	−0.9860	−0.6262	−0.2665	0.0933	0.4531	0.8128	1.1726	1.5323	1.8921
50	−1.7285	−1.4138	−1.0992	−0.7845	−0.4698	−0.1551	0.1596	0.4742	0.7889	1.1036	1.4183
75	−1.7469	−1.4709	−1.1948	−0.9187	−0.6426	−0.3666	−0.0905	0.1856	0.4617	0.7378	1.0138
100	−1.7595	−1.5168	−1.2742	−1.0315	−0.7889	−0.5462	−0.3036	−0.0609	0.1817	0.4243	0.6670
125	−1.7653	−1.5519	−1.3384	−1.1250	−0.9116	−0.6982	−0.4848	−0.2714	−0.0580	0.1555	0.3689
150	−1.7635	−1.5758	−1.3882	−1.2005	−1.0129	−0.8253	−0.6376	−0.4500	−0.2624	−0.0747	0.1129
175	−1.7535	−1.5887	−1.4240	−1.2592	−1.0945	−0.9298	−0.7650	−0.6003	−0.4356	−0.2708	−0.1061
175	−1.2122	−1.0474	−0.8827	−0.7179	−0.5532	−0.3885	−0.2237	−0.0590	0.1057	0.2705	0.4352
200	−1.2223	−1.0780	−0.9337	−0.7895	−0.6452	−0.5010	−0.3567	−0.2124	−0.0682	0.0761	0.2203
225	−1.2201	−1.0942	−0.9684	−0.8425	−0.7167	−0.5909	−0.4650	−0.3392	−0.2134	−0.0875	0.0383
250	−1.2043	−1.0950	−0.9858	−0.8767	−0.7675	−0.6583	−0.5491	−0.4400	−0.3308	−0.2216	−0.1124
275	−1.1740	−1.0798	−0.9858	−0.8917	−0.7977	−0.7036	−0.6096	−0.5156	−0.4215	−0.3275	−0.2335
300	−1.1323	−1.0517	−0.9715	−0.8913	−0.8111	−0.7309	−0.6506	−0.5704	−0.4902	−0.4100	−0.3298
325	−1.0911	−1.0232	−0.9556	−0.8880	−0.8205	−0.7529	−0.6853	−0.6178	−0.5502	−0.4826	−0.4151
350	−1.0824	−1.0259	−0.9700	−0.9141	−0.8582	−0.8022	−0.7463	−0.6904	−0.6345	−0.5785	−0.5226

Table 8.11 Logarithm of the thermodynamic equilibrium constant of reaction (8.10), log $K_{Na-Ca,Cal}$, for pure calcite, adularia, albite, muscovite, and chalcedony (for T < 175 °C) or quartz/chalcedony (for T > 175 °C), as a function of the temperature and the ordering parameter Z of adularia (P = 1 bar for T < 100 °C; P = P_{sat} for T ≥ 100 °C)

T (°C)	Z = 1	Z = 0.9	Z = 0.8	Z = 0.7	Z = 0.6	Z = 0.5	Z = 0.4	Z = 0.3	Z = 0.2	Z = 0.1	Z = 0
0.01	5.3085	5.4462	5.5839	5.7216	5.8593	5.9970	6.1347	6.2724	6.4101	6.5477	6.6854
25	4.3741	4.4940	4.6139	4.7338	4.8537	4.9737	5.0936	5.2135	5.3334	5.4533	5.5733
50	3.6008	3.7057	3.8106	3.9155	4.0204	4.1253	4.2302	4.3350	4.4399	4.5448	4.6497
75	2.9590	3.0510	3.1430	3.2351	3.3271	3.4191	3.5111	3.6032	3.6952	3.7872	3.8792
100	2.4242	2.5051	2.5860	2.6669	2.7478	2.8287	2.9095	2.9904	3.0713	3.1522	3.2331
125	1.9776	2.0487	2.1198	2.1910	2.2621	2.3333	2.4044	2.4755	2.5467	2.6178	2.6889
150	1.6043	1.6669	1.7294	1.7920	1.8545	1.9171	1.9796	2.0422	2.1047	2.1672	2.2298
175	1.2930	1.3479	1.4028	1.4577	1.5126	1.5676	1.6225	1.6774	1.7323	1.7872	1.8421
175	1.8343	1.8892	1.9441	1.9990	2.0539	2.1089	2.1638	2.2187	2.2736	2.3285	2.3834
200	1.5470	1.5951	1.6431	1.6912	1.7393	1.7874	1.8355	1.8836	1.9317	1.9797	2.0278
225	1.3081	1.3501	1.3920	1.4340	1.4759	1.5179	1.5598	1.6018	1.6437	1.6856	1.7276
250	1.1123	1.1487	1.1851	1.2215	1.2579	1.2943	1.3307	1.3671	1.4035	1.4398	1.4762
275	0.9546	0.9861	1.0174	1.0487	1.0801	1.1114	1.1428	1.1741	1.2055	1.2368	1.2682
300	0.8281	0.8550	0.8817	0.9084	0.9352	0.9619	0.9887	1.0154	1.0421	1.0689	1.0956
325	0.7187	0.7414	0.7639	0.7864	0.8090	0.8315	0.8540	0.8765	0.8990	0.9216	0.9441
350	0.5951	0.6140	0.6326	0.6512	0.6699	0.6885	0.7072	0.7258	0.7445	0.7631	0.7817

$$- \frac{780,426}{T^2} + \frac{1523.2}{T} - 0.1345 \tag{8.46}$$

$$\log f_{CO_2,Na-Ca} = \log\left(\frac{a_{Na^+}^2}{a_{Ca^{2+}}}\right) + \left(\frac{579.07}{T} - 0.7430\right) \cdot Z$$
$$- \frac{258,609}{T^2} - \frac{1879.8}{T} + 3.4685 \tag{8.47}$$

$$\log f_{CO_2,Na-Ca} = \log\left(\frac{a_{Na^+}^2}{a_{Ca^{2+}}}\right) + \left(\frac{578.72}{T} - 0.7423\right) \cdot Z$$
$$- \frac{1,081,929}{T^2} + \frac{1648.6}{T} - 0.8608 \tag{8.48}$$

Equations (8.45) and (8.47) are valid below 175 °C, whereas Eqs. (8.46) and (8.48) hold true from 175 to 350 °C. Shifts of muscovite activity of $\pm 1\sigma$ from the mean value determine differences of 0.09–0.12 log-units in the log f_{CO_2} values calculated by means of Eqs. (8.45)–(8.48), irrespective of temperature.

8.5   Derivation of the Theoretical f_{CO_2}-Temperature Functions Controlled by Equilibrium Coexistence of a Ca–Al-Silicate and Calcite

Adopting the same approach described in Sect. 8.4, the log K of reactions (8.11)–(8.14) for pure solid phases were fitted against both the absolute temperature reciprocal and the ordering parameter of adularia, considering separately the data below 175 °C, with chalcedony controlling undissociated SiO_2, and those above 175 °C, with quartz/chalcedony governing undissociated SiO_2. Each regression equation and the average activities of pertinent solid phases were then inserted into Eqs. (8.25)–(8.28). These equations were solved with respect to the logarithm of CO_2 fugacity, thus obtaining four f_{CO_2}-temperature functions, one for each Ca–Al-silicate. Again, the uncertainties brought about by variations in the activities of relevant components in the solid solutions of interest were assessed taking into account the average activities plus one standard deviation and the average activities minus one standard deviation.

8.5.1   The f_{CO_2}-Temperature Functions Fixed by Equilibrium Coexistence of Laumontite and Calcite

The log f_{CO_2} values controlled by laumontite/calcite equilibrium coexistence [see reaction (8.11) and Eq. (8.25)] depend on the absolute temperature reciprocal and the ordering parameter Z of hydrothermal adularia as described by the following relations:

$$\log f_{CO_2} = \left(\frac{579.063}{T} - 0.7430 \right) \cdot Z - \frac{260{,}888}{T^2}$$
$$- \frac{2806.6}{T} + 5.9407 \quad \text{for T} < 175\,^{\circ}\text{C} \tag{8.49}$$

$$\log f_{CO_2} = \left(\frac{578.708}{T} - 0.7422 \right) \cdot Z - \frac{818{,}992}{T^2}$$
$$- \frac{426.78}{T} + 3.0381 \quad \text{for } 175 < \text{T} < 325\,^{\circ}\text{C}. \tag{8.50}$$

Equations (8.49) and (8.50) are based on the log $K_{Lmt\text{-}Cal}$ values shown in Table 8.12. Deviations of muscovite and laumontite activities of $\pm 1\sigma$ from the mean values bring about differences of 0.079–0.104 log-units in the log f_{CO_2} values calculated by means of Eqs. (8.49) and (8.50), irrespective of temperature.

8.5.2   The f_{CO_2}-Temperature Functions Fixed by Equilibrium Coexistence of Clinozoisite and Calcite

The log f_{CO_2} values governed by clinozoisite/calcite equilibrium coexistence [see reaction (8.12) and Eq. (8.26)] vary with the absolute temperature inverse and the ordering parameter Z of hydrothermal adularia as defined by the following equations:

$$\log f_{CO_2} = \left(\frac{434.321}{T} - 0.5573 \right) \cdot Z - \frac{5493.1}{T} + 10.3015 \quad \text{for T} < 175\,^{\circ}\text{C} \tag{8.51}$$

$$\log f_{CO_2} = \left(\frac{434.061}{T} - 0.5568 \right) \cdot Z - \frac{5612.4}{T} + 10.4368$$
$$\text{for } 175 < \text{T} < 325\,^{\circ}\text{C}. \tag{8.52}$$

Equations (8.51) and (8.52) were derived from the log $K_{Czo\text{-}Cal}$ values listed in Table 8.13. Shifts of clinozoisite and muscovite activity of $\pm 1\sigma$ from the mean values cause differences of 0.053–0.070 log-units in the log f_{CO_2} values calculated using Eqs. (8.51) and (8.52), irrespective of temperature.

Table 8.12 Logarithm of the thermodynamic equilibrium constant of reaction (8.11), log $K_{Lmt\text{-}Cal}$, for pure laumontite, calcite, adularia, muscovite, and chalcedony (for T < 175 °C) or quartz/chalcedony (for T > 175 °C), as a function of the temperature and the ordering parameter Z of adularia (P = 1 bar for T < 100 °C; P = P_{sat} for T ≥ 100 °C)

T (°C)	Z = 1	Z = 0.9	Z = 0.8	Z = 0.7	Z = 0.6	Z = 0.5	Z = 0.4	Z = 0.3	Z = 0.2	Z = 0.1	Z = 0
0.01	−6.2868	−6.4245	−6.5622	−6.6999	−6.8376	−6.9753	−7.1130	−7.2506	−7.3883	−7.5260	−7.6637
25	−5.0556	−5.1756	−5.2955	−5.4154	−5.5353	−5.6552	−5.7752	−5.8951	−6.0150	−6.1349	−6.2548
50	−4.0394	−4.1443	−4.2492	−4.3541	−4.4590	−4.5639	−4.6688	−4.7737	−4.8785	−4.9834	−5.0883
75	−3.1919	−3.2840	−3.3760	−3.4680	−3.5601	−3.6521	−3.7441	−3.8361	−3.9282	−4.0202	−4.1122
100	−2.4791	−2.5599	−2.6408	−2.7217	−2.8026	−2.8835	−2.9644	−3.0452	−3.1261	−3.2070	−3.2879
125	−1.8750	−1.9462	−2.0173	−2.0884	−2.1596	−2.2307	−2.3019	−2.3730	−2.4441	−2.5153	−2.5864
150	−1.3604	−1.4229	−1.4855	−1.5480	−1.6105	−1.6731	−1.7356	−1.7982	−1.8607	−1.9233	−1.9858
175	−0.9199	−0.9748	−1.0297	−1.0846	−1.1396	−1.1945	−1.2494	−1.3043	−1.3592	−1.4141	−1.4690
175	−1.2808	−1.3357	−1.3906	−1.4455	−1.5004	−1.5553	−1.6103	−1.6652	−1.7201	−1.7750	−1.8299
200	−0.8835	−0.9316	−0.9797	−1.0278	−1.0759	−1.1240	−1.1720	−1.2201	−1.2682	−1.3163	−1.3644
225	−0.5409	−0.5829	−0.6249	−0.6668	−0.7088	−0.7507	−0.7926	−0.8346	−0.8765	−0.9185	−0.9604
250	−0.2452	−0.2816	−0.3180	−0.3544	−0.3908	−0.4272	−0.4636	−0.5000	−0.5364	−0.5728	−0.6092
275	0.0101	−0.0214	−0.0527	−0.0840	−0.1154	−0.1467	−0.1781	−0.2094	−0.2408	−0.2721	−0.3035
300	0.2300	0.2032	0.1764	0.1497	0.1229	0.0962	0.0695	0.0427	0.0160	−0.0108	−0.0375
325	0.4188	0.3961	0.3736	0.3511	0.3286	0.3060	0.2835	0.2610	0.2385	0.2159	0.1934
350	0.5797	0.5609	0.5423	0.5236	0.5050	0.4863	0.4677	0.4491	0.4304	0.4118	0.3931

Table 8.13 Logarithm of the thermodynamic equilibrium constant of reaction (8.12), log $K_{Czo-Cal}$, for pure clinozoisite, calcite, adularia, muscovite, and chalcedony (for T < 175 °C) or quartz/chalcedony (for T > 175 °C), as a function of the temperature and the ordering parameter Z of adularia (P = 1 bar for T < 100 °C; P = P$_{sat}$ for T ≥ 100 °C)

T (°C)	Z = 1	Z = 0.9	Z = 0.8	Z = 0.7	Z = 0.6	Z = 0.5	Z = 0.4	Z = 0.3	Z = 0.2	Z = 0.1	Z = 0
0.01	−8.7058	−8.8090	−8.9123	−9.0156	−9.1188	−9.2221	−9.3254	−9.4286	−9.5319	−9.6352	−9.7384
25	−7.1625	−7.2524	−7.3424	−7.4323	−7.5223	−7.6122	−7.7021	−7.7921	−7.8820	−7.9720	−8.0619
50	−5.8536	−5.9323	−6.0109	−6.0896	−6.1683	−6.2470	−6.3256	−6.4043	−6.4830	−6.5616	−6.6403
75	−4.7300	−4.7990	−4.8680	−4.9370	−5.0061	−5.0751	−5.1441	−5.2131	−5.2821	−5.3512	−5.4202
100	−3.7550	−3.8157	−3.8763	−3.9370	−3.9977	−4.0583	−4.1190	−4.1797	−4.2403	−4.3010	−4.3616
125	−2.9009	−2.9542	−3.0076	−3.0610	−3.1143	−3.1677	−3.2210	−3.2744	−3.3277	−3.3811	−3.4344
150	−2.1466	−2.1935	−2.2404	−2.2873	−2.3342	−2.3811	−2.4280	−2.4749	−2.5218	−2.5687	−2.6156
175	−1.4754	−1.5166	−1.5578	−1.5990	−1.6402	−1.6814	−1.7226	−1.7637	−1.8049	−1.8461	−1.8873
175	−1.6108	−1.6520	−1.6931	−1.7343	−1.7755	−1.8167	−1.8579	−1.8991	−1.9402	−1.9814	−2.0226
200	−1.0026	−1.0387	−1.0748	−1.1108	−1.1469	−1.1829	−1.2190	−1.2551	−1.2911	−1.3272	−1.3633
225	−0.4547	−0.4862	−0.5176	−0.5491	−0.5806	−0.6120	−0.6435	−0.6749	−0.7064	−0.7379	−0.7693
250	0.0417	0.0143	−0.0130	−0.0403	−0.0676	−0.0949	−0.1221	−0.1494	−0.1767	−0.2040	−0.2313
275	0.4936	0.4701	0.4466	0.4230	0.3995	0.3760	0.3525	0.3290	0.3055	0.2820	0.2585
300	0.9072	0.8871	0.8670	0.8470	0.8269	0.8068	0.7868	0.7667	0.7467	0.7266	0.7066
325	1.2874	1.2704	1.2535	1.2366	1.2197	1.2028	1.1859	1.1691	1.1522	1.1353	1.1184
350	1.6386	1.6245	1.6105	1.5965	1.5825	1.5685	1.5545	1.5406	1.5266	1.5126	1.4986

8.5.3 The f_{CO_2}-Temperature Functions Fixed by Equilibrium Coexistence of Prehnite and Calcite

The log f_{CO_2} values fixed by prehnite/calcite equilibrium coexistence [see reaction (8.13) and Eq. (8.27)] depend on the absolute temperature reciprocal and the ordering parameter Z of hydrothermal adularia according to the following relations:

$$\log f_{CO_2} = \left(\frac{289.504}{T} - 0.3714 \right) \cdot Z - \frac{4369.1}{T} + 8.5567 \quad \text{for T} < 175\,°C \tag{8.53}$$

$$\log f_{CO_2} = \left(\frac{289.321}{T} - 0.3710 \right) \cdot Z - \frac{4372.6}{T} + 8.4261 \quad \text{for } 175 < T < 350\,°C. \tag{8.54}$$

Equations (8.53) and (8.54) were obtained from the log $K_{Prh\text{-}Cal}$ values shown in Table 8.14. Deviations of prehnite and muscovite activity of $\pm1\sigma$ from the average values cause differences of 0.007–0.010 log-units in the log f_{CO_2} values computed using Eqs. (8.53) and (8.54), irrespective of temperature.

8.5.4 The f_{CO_2}-Temperature Functions Fixed by Equilibrium Coexistence of Wairakite and Calcite

The log f_{CO_2} values constrained by wairakite/calcite equilibrium coexistence [see reaction (8.14) and Eq. (8.28)] depend on the absolute temperature inverse and the ordering parameter Z of hydrothermal adularia as described by the following equations:

$$\log f_{CO_2} = \left(\frac{579.066}{T} - 0.7430 \right) \cdot Z - \frac{87,786}{T^2}$$
$$- \frac{6737.3}{T} + 12.7898 \quad \text{for T} < 175\,°C \tag{8.55}$$

$$\log f_{CO_2} = \left(\frac{578.696}{T} - 0.7422 \right) \cdot Z - \frac{416,559}{T^2} - \frac{5422.6}{T} + 11.1262$$
$$\text{for } 175 < T < 350\,°C. \tag{8.56}$$

Equations (8.55) and (8.56) were derived from the log $K_{Wrk\text{-}Cal}$ values listed in Table 8.15. Shifts of wairakite and muscovite activity of $\pm1\sigma$ from the average values cause differences of 0.051–0.072 log-units in the log f_{CO_2} values computed using Eqs. (8.55) and (8.56), independent of temperature.

Table 8.14 Logarithm of the thermodynamic equilibrium constant of reaction (8.13), log $K_{Prh-Cal}$, for pure prehnite, calcite, adularia, muscovite, and chalcedony (for T < 175 °C) or quartz/chalcedony (for T > 175 °C), as a function of the temperature and the ordering parameter Z of adularia (P = 1 bar for T < 100 °C; P = P_{sat} for T ≥ 100 °C)

T (°C)	Z = 1	Z = 0.9	Z = 0.8	Z = 0.7	Z = 0.6	Z = 0.5	Z = 0.4	Z = 0.3	Z = 0.2	Z = 0.1	Z = 0
0.01	−6.7200	−6.7888	−6.8577	−6.9265	−6.9954	−7.0642	−7.1331	−7.2019	−7.2707	−7.3396	−7.4084
25	−5.4646	−5.5245	−5.5845	−5.6444	−5.7044	−5.7644	−5.8243	−5.8843	−5.9442	−6.0042	−6.0642
50	−4.4034	−4.4559	−4.5083	−4.5608	−4.6132	−4.6657	−4.7181	−4.7706	−4.8230	−4.8754	−4.9279
75	−3.4957	−3.5418	−3.5878	−3.6338	−3.6798	−3.7258	−3.7718	−3.8178	−3.8638	−3.9099	−3.9559
100	−2.7110	−2.7515	−2.7919	−2.8324	−2.8728	−2.9132	−2.9537	−2.9941	−3.0346	−3.0750	−3.1155
125	−2.0261	−2.0617	−2.0973	−2.1328	−2.1684	−2.2040	−2.2396	−2.2751	−2.3107	−2.3463	−2.3818
150	−1.4235	−1.4548	−1.4861	−1.5173	−1.5486	−1.5799	−1.6112	−1.6424	−1.6737	−1.7050	−1.7363
175	−0.8894	−0.9169	−0.9443	−0.9718	−0.9992	−1.0267	−1.0542	−1.0816	−1.1091	−1.1365	−1.1640
175	−1.0247	−1.0522	−1.0797	−1.1071	−1.1346	−1.1620	−1.1895	−1.2169	−1.2444	−1.2719	−1.2993
200	−0.5411	−0.5651	−0.5892	−0.6132	−0.6373	−0.6613	−0.6853	−0.7094	−0.7334	−0.7575	−0.7815
225	−0.1069	−0.1279	−0.1489	−0.1699	−0.1908	−0.2118	−0.2328	−0.2537	−0.2747	−0.2957	−0.3167
250	0.2849	0.2667	0.2485	0.2303	0.2121	0.1939	0.1757	0.1575	0.1393	0.1212	0.1030
275	0.6405	0.6248	0.6091	0.5934	0.5777	0.5621	0.5464	0.5307	0.5150	0.4994	0.4837
300	0.9646	0.9512	0.9378	0.9244	0.9111	0.8977	0.8843	0.8710	0.8576	0.8442	0.8308
325	1.2615	1.2502	1.2389	1.2276	1.2164	1.2051	1.1938	1.1826	1.1713	1.1601	1.1488
350	1.5347	1.5253	1.5159	1.5066	1.4973	1.4880	1.4787	1.4693	1.4600	1.4507	1.4414

Table 8.15 Logarithm of the thermodynamic equilibrium constant of reaction (8.14), log $K_{Wrk-Cal}$, for pure wairakite, calcite, adularia, muscovite, and chalcedony (for T < 175 °C) or quartz/chalcedony (for T > 175 °C), as a function of the temperature and the ordering parameter Z of adularia (P = 1 bar for T < 100 °C; P = P_{sat} for T ≥ 100 °C)

T (°C)	Z = 1	Z = 0.9	Z = 0.8	Z = 0.7	Z = 0.6	Z = 0.5	Z = 0.4	Z = 0.3	Z = 0.2	Z = 0.1	Z = 0
0.01	−11.5366	−11.6743	−11.8120	−11.9497	−12.0874	−12.2250	−12.3627	−12.5004	−12.6381	−12.7758	−12.9135
25	−9.4651	−9.5850	−9.7049	−9.8249	−9.9448	−10.0647	−10.1846	−10.3045	−10.4245	−10.5444	−10.6643
50	−7.7195	−7.8244	−7.9292	−8.0341	−8.1390	−8.2439	−8.3488	−8.4537	−8.5586	−8.6635	−8.7684
75	−6.2313	−6.3233	−6.4154	−6.5074	−6.5994	−6.6914	−6.7835	−6.8755	−6.9675	−7.0595	−7.1516
100	−4.9496	−5.0305	−5.1113	−5.1922	−5.2731	−5.3540	−5.4349	−5.5158	−5.5966	−5.6775	−5.7584
125	−3.8360	−3.9071	−3.9783	−4.0494	−4.1206	−4.1917	−4.2628	−4.3340	−4.4051	−4.4762	−4.5474
150	−2.8610	−2.9236	−2.9861	−3.0487	−3.1112	−3.1738	−3.2363	−3.2989	−3.3614	−3.4239	−3.4865
175	−2.0017	−2.0567	−2.1116	−2.1665	−2.2214	−2.2763	−2.3312	−2.3861	−2.4410	−2.4960	−2.5509
175	−2.3626	−2.4175	−2.4724	−2.5274	−2.5823	−2.6372	−2.6921	−2.7470	−2.8019	−2.8568	−2.9117
200	−1.5818	−1.6299	−1.6780	−1.7261	−1.7742	−1.8223	−1.8703	−1.9184	−1.9665	−2.0146	−2.0627
225	−0.8860	−0.9279	−0.9699	−1.0118	−1.0538	−1.0957	−1.1377	−1.1796	−1.2216	−1.2635	−1.3054
250	−0.2631	−0.2995	−0.3359	−0.3723	−0.4087	−0.4451	−0.4815	−0.5179	−0.5543	−0.5907	−0.6271
275	0.2966	0.2652	0.2338	0.2025	0.1711	0.1398	0.1084	0.0771	0.0457	0.0144	−0.0170
300	0.8011	0.7742	0.7475	0.7208	0.6940	0.6673	0.6405	0.6138	0.5871	0.5603	0.5336
325	1.2571	1.2344	1.2119	1.1894	1.1669	1.1444	1.1218	1.0993	1.0768	1.0543	1.0318
350	1.6701	1.6513	1.6327	1.6140	1.5954	1.5767	1.5581	1.5394	1.5208	1.5022	1.4835

8.6 Plots of the K^2/Ca- and Na^2/Ca-Log Activity Ratios Versus the Absolute Temperature Inverse

The reservoir liquids of interest as well as the theoretical K–Ca and Na–Ca geother-mometers and f_{CO_2}-indicators which were derived in Sect. 8.4 are shown in the diagrams of Figs. 8.1, 8.2, 8.3, 8.4, 8.5 and 8.6. The reservoir liquids are indi-cated by the usual symbols, whereas the K–Ca and Na–Ca theoretical geoindicators are represented by lines of different color, namely moss-green for the laumontite geothermometers, green for the clinozoisite geothermometers, orange for the prehnite geothermometers, olive for the wairakite geothermometers, and grey for the calcite f_{CO_2}-indicators, whose lines refer to different f_{CO_2} values, as specified.

For the geoindicators involving the ordering parameter of adularia, Z was alter-natively set at 0.30 (mean value -1σ, dashed lines) and 0.82 (mean value $+1\sigma$, solid lines) to bracket the range of Z values of most hydrothermal adularias in hypothet-ical equilibrium with the considered reservoir liquids (see Sect. 6.1). The activities of Ca-endmembers in Ca–Al-silicates and of muscovite in illite were assumed equal to the average values for the hydrothermal solid solutions from active geothermal systems (see Sect. 8.2), like in the derivation of the geoindicators (Sect. 8.4).

For the calcite f_{CO_2}-indicator, at the same f_{CO_2} value, the theoretical K^2/Ca-log activity ratios of the aqueous solution for Z = 0.30 and Z = 0.82 differ by 1.26 log-units at 100 °C, 0.75 log-units at 200 °C, and 0.42 log-units at 300 °C, whereas the differences in the theoretical Na^2/Ca-log activity ratios are 1/3 of previous figures,
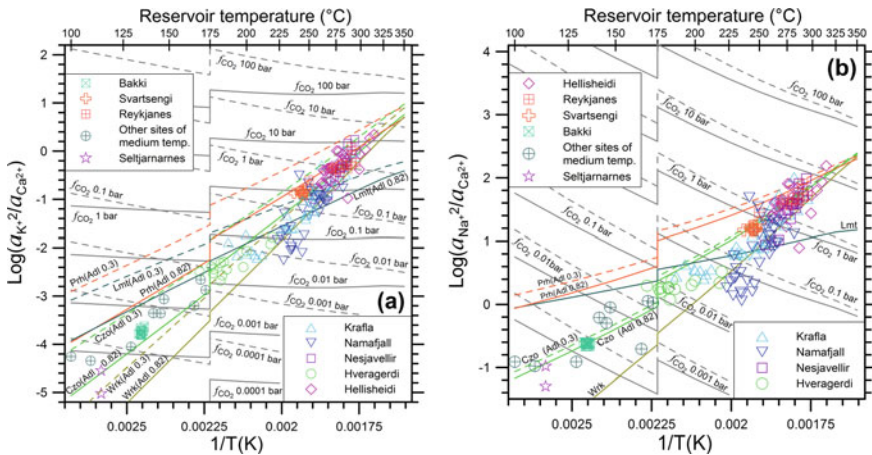
Fig. 8.1 Logarithm of the **a** K^2/Ca and **b** Na^2/Ca activity ratios of the selected reservoir liquids from the geothermal fields of Iceland as a function of the aquifer temperature reciprocal. Also shown are the theoretical log activity ratios fixed by mineral-solution equilibria, for average activities of relevant solid phases. Different f_{CO_2} values, as indicated, were considered for the reactions involving calcite (gray lines). The ordering parameter of adularia was set at 0.30 (dashed lines) and 0.82 (solid lines), to bracket the range of Z values of adularia apparently in equilibrium with the reservoir liquids of interest
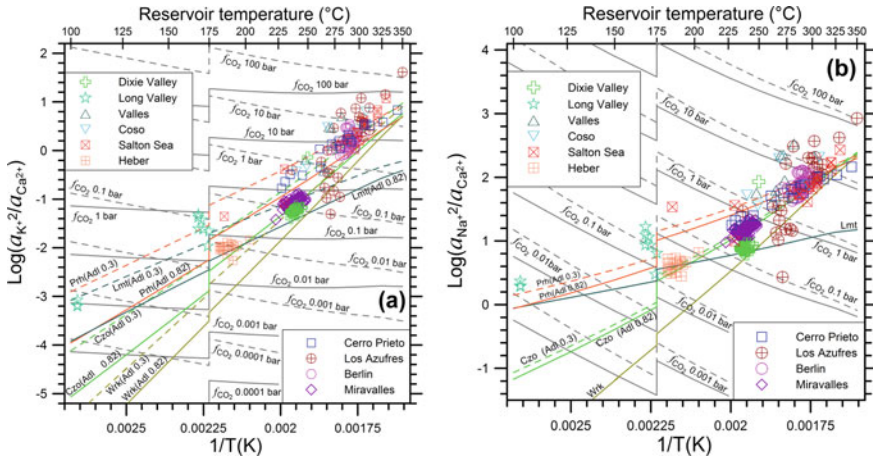
Fig. 8.2 Logarithm of the **a** K^2/Ca and **b** Na^2/Ca activity ratios of the selected reservoir liquids from the geothermal fields of Northern and Central America as a function of the aquifer temperature reciprocal. Also shown are the theoretical log activity ratios fixed by mineral-solution equilibria, for average activities of relevant solid phases. Different f_{CO_2} values, as indicated, were considered for the reactions involving calcite (gray lines). The ordering parameter of adularia was set at 0.30 (dashed lines) and 0.82 (solid lines), to bracket the range of Z values of adularia apparently in equilibrium with the reservoir liquids of interest
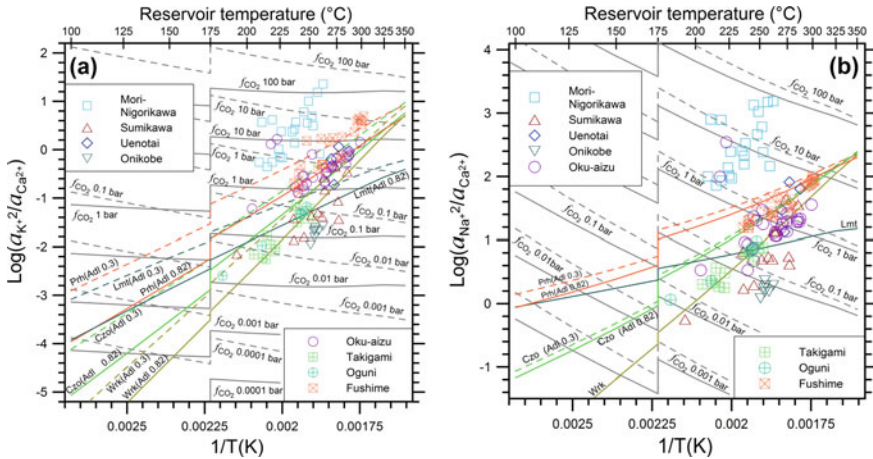
Fig. 8.3 Logarithm of the **a** K^2/Ca and **b** Na^2/Ca activity ratios of the selected reservoir liquids from the geothermal fields of Japan as a function of the aquifer temperature reciprocal. Also shown are the theoretical log activity ratios fixed by mineral-solution equilibria, for average activities of relevant solid phases. Different f_{CO_2} values, as indicated, were considered for the reactions involving calcite (gray lines). The ordering parameter of adularia was set at 0.30 (dashed lines) and 0.82 (solid lines), to bracket the range of Z values of adularia apparently in equilibrium with the reservoir liquids of interest
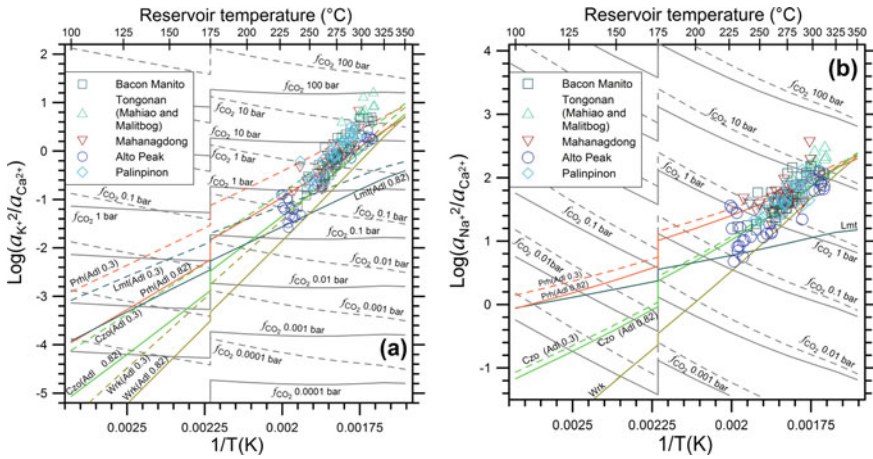
Fig. 8.4 Logarithm of the **a** K^2/Ca and **b** Na^2/Ca activity ratios of the selected reservoir liquids from the geothermal fields of the Philippines as a function of the aquifer temperature reciprocal. Also shown are the theoretical log activity ratios fixed by mineral-solution equilibria, for average activities of relevant solid phases. Different f_{CO_2} values, as indicated, were considered for the reactions involving calcite (gray lines). The ordering parameter of adularia was set at 0.30 (dashed lines) and 0.82 (solid lines), to bracket the range of Z values of adularia apparently in equilibrium with the reservoir liquids of interest
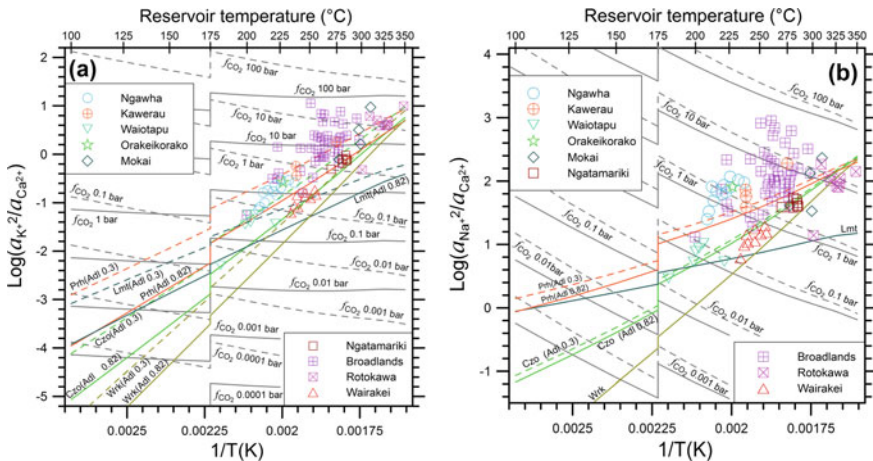
Fig. 8.5 Logarithm of the **a** K^2/Ca and **b** Na^2/Ca activity ratios of the selected reservoir liquids from the geothermal fields of New Zealand as a function of the aquifer temperature reciprocal. Also shown are the theoretical log activity ratios fixed by mineral-solution equilibria, for average activities of relevant solid phases. Different f_{CO_2} values, as indicated, were considered for the reactions involving calcite (gray lines). The ordering parameter of adularia was set at 0.30 (dashed lines) and 0.82 (solid lines), to bracket the range of Z values of adularia apparently in equilibrium with the reservoir liquids of interest
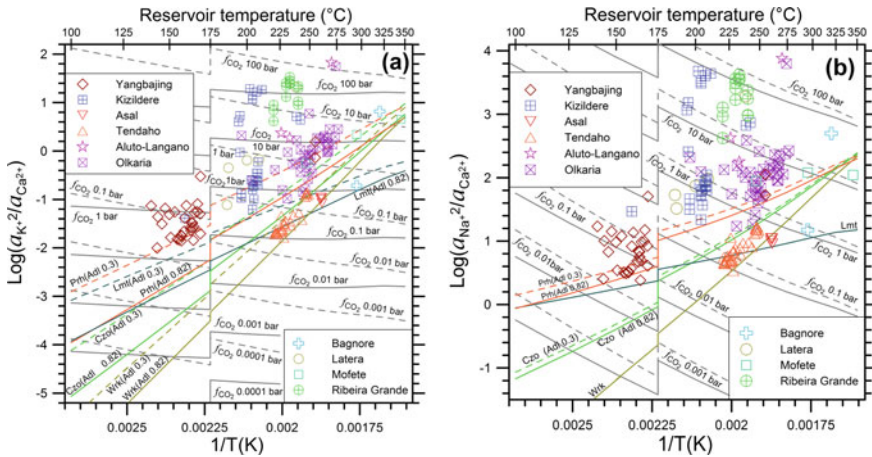
Fig. 8.6 Logarithm of the **a** K^2/Ca and **b** Na^2/Ca activity ratios of the selected reservoir liquids from miscellaneous geothermal fields as a function of the aquifer temperature reciprocal. Also shown are the theoretical log activity ratios fixed by mineral-solution equilibria, for average activities of relevant solid phases. Different f_{CO_2} values, as indicated, were considered for the reactions involving calcite (gray lines). The ordering parameter of adularia was set at 0.30 (dashed lines) and 0.82 (solid lines), to bracket the range of Z values of adularia apparently in equilibrium with the reservoir liquids of interest

being 0.42 log-units at 100 °C, 0.25 log-units at 200 °C, and 0.14 log-units at 300 °C. This different impact of adularia order-disorder is due to its different stoichiometric coefficient, which is 3 in the K–Ca exchange reaction (8.9) controlling the K^2/Ca activity ratio, but is 1 in Na–Ca exchange reaction (8.10), governing the Na^2/Ca activity ratio.

Likewise, for the reactions comprising Ca–Al silicates, adularia order-disorder has a greater impact on the theoretical K^2/Ca-log activity ratios than on the corresponding Na^2/Ca-log activity ratios. Again, these differences are related to the higher stoichiometric coefficient of adularia in the K–Ca exchange reactions (8.1), (8.2), (8.3), and (8.4), compared to the Na–Ca exchange reactions (8.5), (8.6), (8.7), and (8.8), respectively. In particular, the theoretical Na^2/Ca-log activity ratios governed by the Na–Ca exchange reactions (8.5) and (8.8), involving laumontite and wairakite, respectively, do not depend on Z because adularia does not participate to these reactions.

In the plots of the K^2/Ca log-activity ratio versus the aquifer temperature reciprocal as well as in the diagrams of the Na^2/Ca log-activity ratio versus the aquifer temperature inverse, the lines of the wairakite, clinozoisite and prehnite geothermometers converge gradually with increasing temperatures and diverge progressively with decreasing temperatures, whereas the lines of the laumontite geothermometers have lower slope and cross the lines of the wairakite, clinozoisite and prehnite geothermometers. Consequently, for the reservoir liquids of medium-low temperature (in the range 100–200 °C approximately), the attainment of equilibrium with either prehnite

or clinozoisite or wairakite results in substantially different K^2/Ca and Na^2/Ca log-activity ratios, at any given temperature and Z value of adularia. In other words, in principle, it is possible to establish if a given low-temperature reservoir liquid is in equilibrium with either prehnite or clinozoisite or wairakite. However, there are some ambiguities owing to the possible attainment of equilibrium with laumontite instead of prehnite or clinozoisite.

In contrast, the high-temperature reservoir liquids may appear to be in equilibrium (or close to it) with two or even three Ca–Al-silicates at the same time, which is obviously an impossible condition because it would violate the Gibbs' phase rule. This apparent multiple-equilibrium condition is due to the small differences in the Gibbs free energies and log K values of the K–Ca and Na–Ca exchange reactions involving prehnite, clinozoisite, and wairakite above 200 °C approximately. Furthermore, the differences between the Gibbs free energies of these reactions become smaller and smaller with increasing temperature.

The reservoir liquids of interest can be separated into three different groups based on their position with respect to the lines of the Ca–Al-silicate geothermometers in the diagrams of Figs. 8.1, 8.2, 8.3, 8.4, 8.5 and 8.6, namely those situated along these lines, those that are found above these lines and those that are located below these lines.

Most reservoir liquids from the geothermal fields of Iceland (Fig. 8.1), Northern and Central America (Fig. 8.2), and the Philippines (Fig. 8.4), as well as the Japanese reservoir liquids from Uenotai, Takigami, Oguni, and Fushime (Fig. 8.3), the New Zealand reservoir liquids from Waiotapu, Ngatamariki, Rotokawa, and Wairakei (Fig. 8.5), and those from Asal and Tendaho (Fig. 8.6) are positioned in the area below the dashed line of the prehnite geothermometers and above the solid lines of the wairakite and laumontite geothermometers (intersecting at ~250 °C), indicating that these reservoir liquids are in equilibrium with a Ca–Al-silicate or close to this condition. Therefore, the K^2/Ca and Na^2/Ca log-activity ratios of these reservoir liquids can be inserted into the geothermometric functions controlled by laumontite, Eqs. (8.29)–(8.32), clinozoisite, Eqs. (8.33)–(8.36), prehnite, Eqs. (8.37)–(8.40), and wairakite, Eqs. (8.41)–(8.44), to compute the temperatures possibly occurring in the geothermal reservoir.

Several reservoir liquids are situated above the dashed line of the prehnite geothermometers and are in apparent equilibrium with calcite, under the CO_2 fugacity values indicated by the grey lines. This is the case of all the reservoir liquids from Mori-Nigorikawa (Fig. 8.3), Ngawha, Orakeikorako, and Kawerau (Fig. 8.5), Kizildere, Ribeira Grande, Aluto-Langano, and Latera (Fig. 8.6). Moreover, most reservoir liquids from Long Valley and some from Valles, Coso, and Los Azufres (Fig. 8.2), a few from The Philippines geothermal fields (Fig. 8.4), several from Broadlands (Fig. 8.5), Yangbajing and Olkaria (Fig. 8.6) are also in apparent equilibrium with calcite. The word apparent is necessary, because the K^2/Ca and Na^2/Ca log-activity ratios of these reservoir liquids could be affected by Ca loss due to precipitation of calcite or other Ca-bearing solid phases. If this is not the case, the K^2/Ca and Na^2/Ca log-activity ratios of these reservoir liquids can be inserted into Eqs. (8.45)–(8.48) to calculate the f_{CO_2} presumably present in the geothermal aquifer.

Below the solid lines of the wairakite and laumontite geothermometers (inter-secting at ~250 °C) there are only few sample points, including all the reservoir liquids from Onikobe, some from Sumikawa (Fig. 8.3), some from Namafjall (Fig. 8.1), and one from Los Azufres (Fig. 8.2). The low K^2/Ca and Na^2/Ca log-activity ratios of these aqueous solutions might be due to rock dissolution promoted by their initial acidity, causing preferential acquisition of Ca, as proposed by Truesdell and Nakan-ishi (2005) for Onikobe. Accepting this interpretation, these reservoir liquids are probably in disequilibrium with both Ca–Al-silicates and calcite and cannot be used to compute neither the temperature nor the CO_2 fugacity of the geothermal aquifer.

8.7   Plots of CO_2 Fugacity Versus the Absolute Temperature Inverse

The theoretical K–Ca and Na–Ca calcite f_{CO_2}-indicators, that is Eqs. (8.45)–(8.48) provide the same CO_2 fugacities, with deviations varying from 0.00019 to 1.7% with respect to the average f_{CO_2} values. These deviations increase with decreasing f_{CO_2} and are ascribable to numerical approximations. Therefore, it is permissible to average the results of the K–Ca and Na–Ca calcite f_{CO_2}-indicators. Strictly speaking, the use of these f_{CO_2}-indicators is not correct for the reservoir liquids in equilibrium with Ca–Al-silicates, because these reservoir liquids are not in equilibrium with calcite. Nevertheless, this action is tolerable, since it is likely that these reservoir liquids are not too far from calcite saturation.

The f_{CO_2} values of the selected reservoir liquids, obtained by averaging the results of the K–Ca and Na–Ca calcite f_{CO_2}-indicators, as well as the four theoretical f_{CO_2}-temperature functions controlled by equilibrium coexistence of a Ca–Al-silicate and calcite (which were derived in Sect. 8.5) are reported in the diagrams of CO_2 fugacity (on a logarithmic scale) versus the reservoir temperature inverse of Figs. 8.7, 8.8 and 8.9. Also in these diagrams, the reservoir liquids are represented by the usual symbols, whereas the f_{CO_2}-temperature functions are indicated by lines of the same colors adopted in Figs. 8.1, 8.2, 8.3, 8.4, 8.5 and 8.6, namely moss-green for the laumontite-calcite functions, green for the clinozoisite-calcite functions, orange for the prehnite-calcite functions, and olive for the wairakite-calcite functions.

Again, the ordering parameter of adularia was assumed equal to 0.30 (dashed lines) or 0.82 (solid lines) to bracket the range of Z values of hydrothermal adularias apparently in equilibrium with the considered reservoir liquids (see Sect. 6.1). The activities of relevant endmembers in the solid solutions of interest, that is muscovite in illite, laumontite in laumontite/alkali-laumontite, clinozoisite in clinozoisite/epidote, prehnite in prehnite/ferri-prehnite, and wairakite in wairakite/analcime, were assumed equal to the average values for the hydrothermal minerals from active geothermal systems (see Sect. 8.2), like in the derivation of the theoretical f_{CO_2}-temperature functions controlled by equilibrium coexistence of a Ca-Al-silicate and calcite (Sect. 8.5).
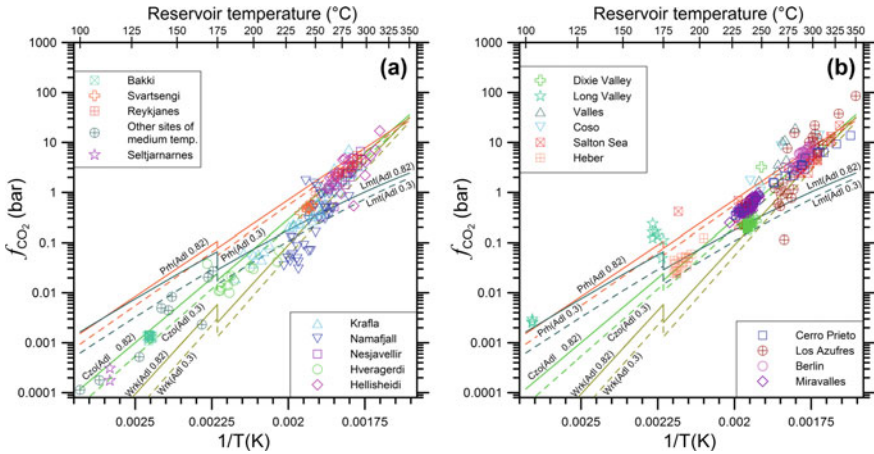
Fig. 8.7 Diagram of CO_2 fugacity (on a logarithmic scale) computed by averaging the results of the K–Ca and Na–Ca calcite f_{CO_2}-indicators versus the reservoir temperature inverse for the selected reservoir liquids from the geothermal fields of **a** Iceland and **b** Northern and Central America. Also shown are the lines of equilibrium coexistence of calcite and a Ca–Al-silicate, drawn for the ordering parameter of adularia $Z = 0.82$ (solid lines) and $Z = 0.30$ (dashed lines), assuming average activities of relevant solid phases
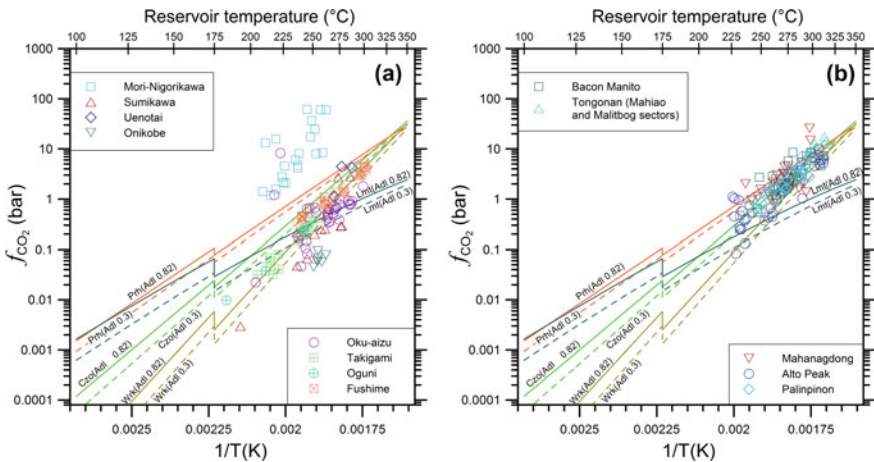
Fig. 8.8 Diagram of CO_2 fugacity (on a logarithmic scale) computed by averaging the results of the K–Ca and Na–Ca calcite f_{CO_2}-indicators versus the reservoir temperature inverse for the selected reservoir liquids from the geothermal fields of **a** Japan and **b** The Philippines. Also shown are the lines of equilibrium coexistence of calcite and a Ca–Al-silicate, drawn for the ordering parameter of adularia $Z = 0.82$ (solid lines) and $Z = 0.30$ (dashed lines), assuming average activities of relevant solid phases
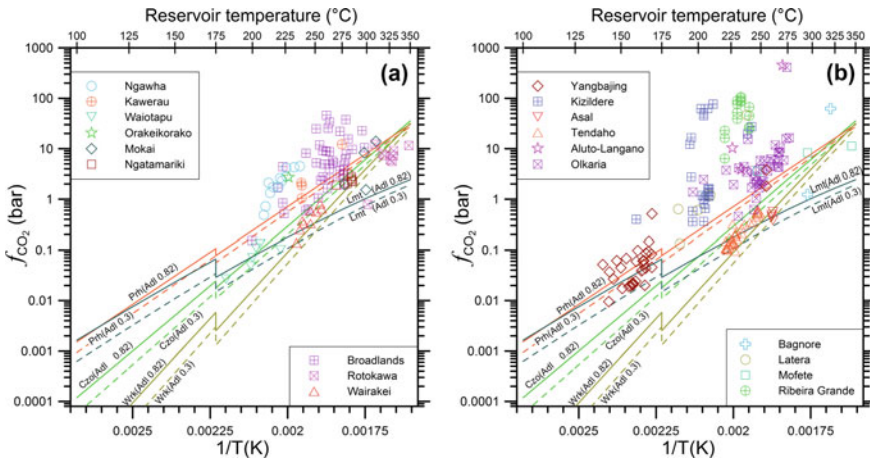
Fig. 8.9 Diagram of CO_2 fugacity (on a logarithmic scale) computed by averaging the results of the K–Ca and Na–Ca calcite f_{CO_2}-indicators versus the reservoir temperature inverse for the selected reservoir liquids from the geothermal fields of **a** New Zealand and **b** miscellaneous sites. Also shown are the lines of equilibrium coexistence of calcite and a Ca–Al-silicate, drawn for the ordering parameter of adularia Z = 0.82 (solid lines) and Z = 0.30 (dashed lines), assuming average activities of relevant solid phases

Similar to what was observed in the plots of Figs. 8.1, 8.2, 8.3, 8.4, 8.5 and 8.6, also in the diagrams of Figs. 8.7, 8.8 and 8.9, the log f_{CO_2}-temperature functions constrained by equilibrium coexistence of calcite and wairakite, calcite and clinozoisite, and calcite and prehnite converge progressively with increasing temperatures and diverge gradually with decreasing temperatures, whereas the two functions fixed by equilibrium coexistence of calcite and laumontite have lower slope and intersect the other calcite/Ca–Al-silicates functions.

Not surprisingly, sample points are distributed in the plots of Figs. 8.7, 8.8 and 8.9 similar to what is observed in Figs. 8.1, 8.2, 8.3, 8.4, 8.5 and 8.6. In fact:

1. The reservoir liquids situated along the lines of the Ca–Al-silicate geothermometers in the plots of Figs. 8.1, 8.2, 8.3, 8.4, 8.5 and 8.6 are found along the lines constrained by equilibrium coexistence of calcite and a Ca–Al-silicate in the diagrams of Figs. 8.7, 8.8 and 8.9, confirming their condition of equilibrium with one of the considered Ca–Al-silicates.
2. The reservoir liquids positioned above the lines of the Ca–Al-silicate geothermometers in the plots of Figs. 8.1, 8.2, 8.3, 8.4, 8.5 and 8.6 are encountered above the lines constrained by equilibrium coexistence of calcite and a Ca–Al-silicate in the diagrams of Figs. 8.7, 8.8 and 8.9, confirming their condition of equilibrium with calcite.
3. The few reservoir liquids located below the lines of the Ca–Al-silicate geothermometers, in the plots of Figs. 8.1, 8.2, 8.3, 8.4, 8.5 and 8.6 are found below the lines constrained by equilibrium coexistence of calcite and a Ca–Al-silicate

in the diagrams of Figs. 8.7, 8.8 and 8.9, being in disequilibrium with both Ca–Al-silicates and calcite.

All in all, the similarity in the distribution of sample points in the two series of diagrams is expected, but the additional information provided by the diagrams of Figs. 8.7, 8.8 and 8.9 is the distinction among: (a) The reservoir liquids in equilibrium with a Ca–Al-silicate, to which it is permissible to apply the theoretical K–Ca and Na–Ca geothermometers derived in Sect. 8.4, that is Eqs. (8.29)–(8.44), to compute the temperatures possibly occurring in the geothermal reservoir. (b) The reservoir liquids in equilibrium with calcite, which are suitable for using the theoretical K–Ca and Na–Ca calcite f_{CO_2}-indicators, i.e., Eqs. (8.45)–(8.48), to calculate the f_{CO_2} presumably present in the geothermal aquifer. (c) The reservoir liquids in disequilibrium with both Ca–Al-silicates and calcite, which cannot be used to compute neither the temperature nor the CO$_2$ fugacity of the geothermal aquifer.

8.8 Use of the K–Ca and Na–Ca Activity-Based Theoretical Geoindicators

The diagrams examined in Sects. 8.6 and 8.7 provide an useful overview. However, it is necessary to decide for each individual reservoir liquid if its K^2/Ca and Na^2/Ca log-activity ratios can be used to estimate the temperature or the CO$_2$ fugacity of the geothermal aquifer. To this purpose, it is advisable to compare the CO$_2$ fugacity computed by averaging the results of the K–Ca and Na–Ca calcite f_{CO_2}-indicators, that is Eqs. (8.45)–(8.48), with the maximum CO$_2$ fugacity given by the f_{CO_2}-temperature functions controlled by equilibrium coexistence of a Ca–Al-silicate and calcite, that is Eqs. (8.49)–(8.56). If the average CO$_2$ fugacity given by the K–Ca and Na–Ca calcite f_{CO_2}-indicators is higher than the maximum CO$_2$ fugacity of Ca–Al-silicate/calcite equilibrium coexistence, then the reservoir liquid can be assumed to be in saturation with calcite, and the computed CO$_2$ fugacity can be considered reliable and representative of the geothermal aquifer. If the opposite is true, then the reservoir liquid can be assumed to be in equilibrium with a Ca–Al silicate and the different theoretical K–Ca and Na–Ca geothermometers can be applied to it.

We tested this approach using the 1013 reservoir liquids of interest. Results are presented and discussed here below. First, the 23 reservoir liquids presumably in disequilibrium with both Ca–Al-silicates and calcite, being situated below the lines of the Ca–Al-silicate geothermometers, and the Sumikawa sample SM-2_78, with Ca concentration lower than detection limit, were excluded from further processing. The 24 excluded reservoir liquids comprise 8 entries of Namafjall, 1 of Los Azufres, 8 of Sumikawa, and 7 of Onikobe.

Among the remaining 990 reservoir liquids, 706 are suitable for using the theoretical K–Ca and Na–Ca geothermometers, whereas 283 are appropriate for utilizing the theoretical K–Ca and Na–Ca f_{CO_2}-indicators. The computed temperatures and

related errors are discussed in Sect. 8.8.1, whereas the calculated CO_2 fugacities and associated uncertainties are presented in Sect. 8.8.2.

8.8.1 Temperatures Given by the Theoretical, Activity-Based K–Ca and Na–Ca Geothermometers and Related Uncertainties

For each reservoir liquid suitable for geothermometry, four K–Ca temperatures and four Na–Ca temperatures were computed. Among them, the K–Ca and Na–Ca temperatures closest to each aquifer temperature were adopted, maintaining the information on the Ca–Al-silicate mineral controlling the geothermometer(s) used to calculate these adopted temperatures. The adopted K–Ca and Na–Ca temperatures are contrasted with the aquifer temperature in the diagrams of Figs. 8.10, 8.11, 8.12, and 8.13, referring to the clinozoisite, wairakite, laumontite, and prehnite geothermometers.

As a whole, the error on the adopted K-Ca temperatures (i.e., the absolute value of their deviation from the aquifer temperature) ranges between 0.0 and 16.9 °C, with an average of 3.8 °C, a median of 3.0 °C and a standard deviation of 3.0 °C. The errors on the adopted K–Ca temperatures are ≤5 °C in 519 cases (73.5% of the total), >5 and ≤10 °C in 168 cases (23.8% of the total), and >10 °C in 19 cases (2.7% of the total).

The error on the adopted Na–Ca temperatures varies between 0 and 36.9 °C, with a mean of 6.9 °C, a median of 6.0 °C and a standard deviation of 5.3 °C. The errors on the adopted Na–Ca temperatures are ≤5 °C in 332 cases (47.0% of the total),
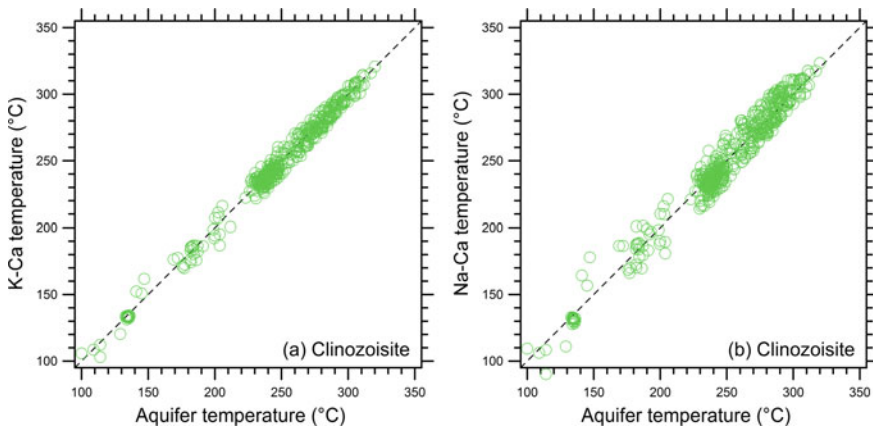
Fig. 8.10 Diagram of the aquifer temperature versus the adopted **a** K–Ca and **b** Na–Ca clinozoisite temperatures
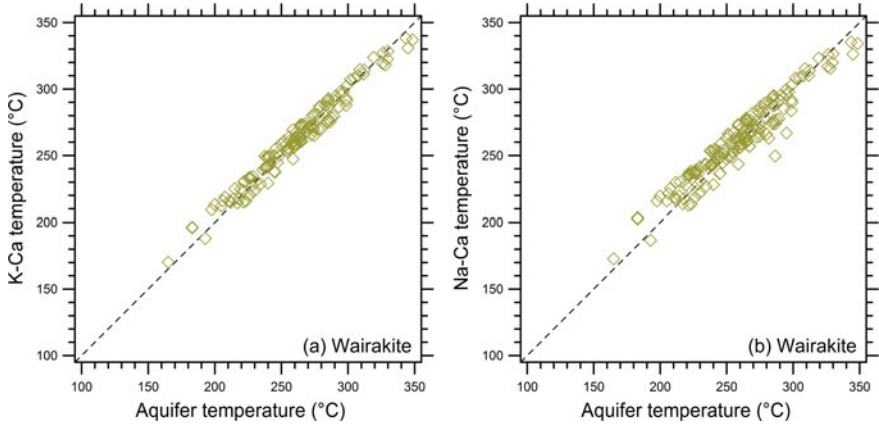
Fig. 8.11 Diagram of the aquifer temperature versus the adopted **a** K–Ca and **b** Na–Ca wairakite temperatures
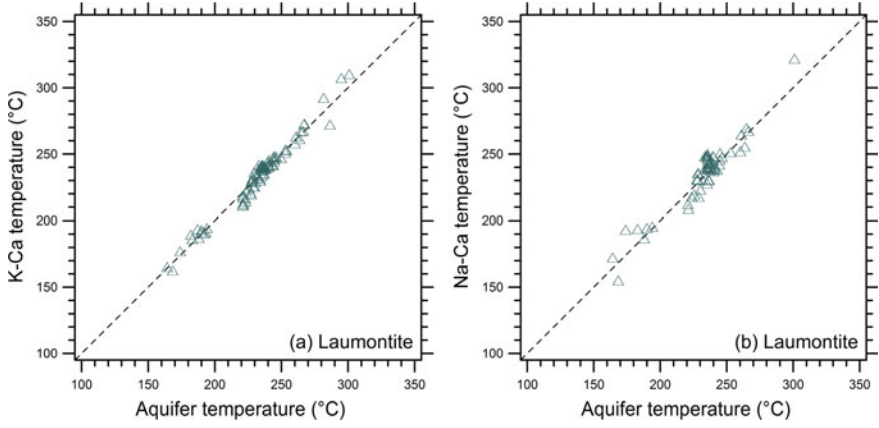
Fig. 8.12 Diagram of the aquifer temperature versus the adopted **a** K–Ca and **b** Na–Ca laumontite temperatures

>5 °C and ≤10 °C in 201 cases (28.5% of the total), >10 °C and ≤15 °C in 127 cases (18.0% of the total), and >15 °C in 46 cases (6.5% of the total).

The adopted K–Ca temperatures include 421 clinozoisite temperatures, 141 wairakite temperatures, 93 laumontite temperatures, and 51 prehnite temperatures. The adopted Na–Ca temperatures include 459 clinozoisite temperatures, 169 wairakite temperatures, 63 laumontite temperatures, and 15 prehnite temperatures. The concordant cases (i.e., the adopted K–Ca and Na–Ca temperatures refer to the same Ca–Al-silicate mineral) are 634, corresponding to 90% of the total, whereas the discordant cases (i.e., the adopted K–Ca and Na–Ca temperatures refer to distinct
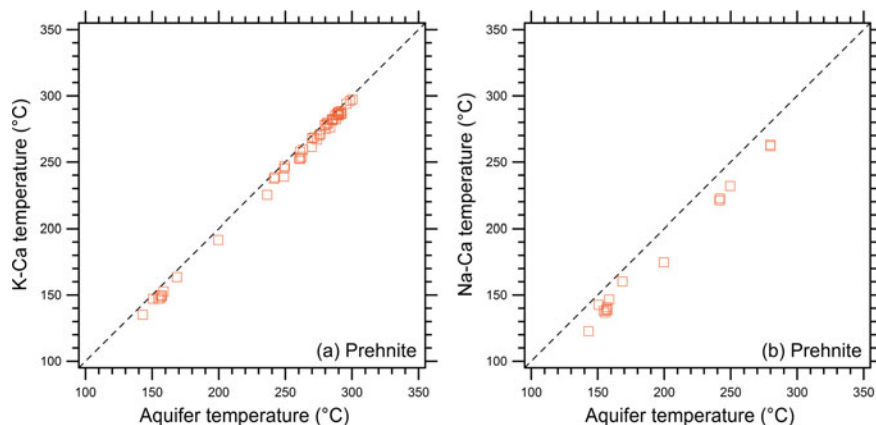
Fig. 8.13 Diagram of the aquifer temperature versus the adopted **a** K–Ca and **b** Na–Ca prehnite temperatures

Ca–Al-silicate minerals) are 72, equivalent to 10% of the total, which is an acceptably low value.

The 421 K–Ca clinozoisite temperatures vary from 103 to 321 °C, with an average of 248 °C, a median of 258 °C, and a standard deviation of 81 °C. The error on the K–Ca clinozoisite temperatures ranges between 0 and 17 °C, with a mean of 3.4 °C, a median of 6.0 °C, and a standard deviation of 7.1 °C.

The 141 K–Ca wairakite temperatures range from 170 to 338 °C with a mean of 262 °C, a median of 263 °C, and a standard deviation of 33 °C. The error on the K–Ca wairakite temperatures varies between 0 and 14 °C, with an average of 5.0 °C, a median of 5.0 °C, and a standard deviation of 3.5 °C.

The 93 K–Ca laumontite temperatures vary from 163 to 310 °C, with an average of 234 °C, a median of 239 °C, and a standard deviation of 26 °C. The error on the K–Ca laumontite temperatures ranges between 0 and 14 °C, with a mean of 3.2 °C, a median of 2.0 °C, and a standard deviation of 2.9 °C.

The 51 K–Ca prehnite temperatures range from 135 to 297 °C, with a mean of 249 °C, a median of 239 °C, and a standard deviation of 67 °C. The error on the K–Ca prehnite temperatures varies between 0 and 11 °C, with an average of 4.5 °C, a median of 6.5 °C, and a standard deviation of 2.1 °C.

The 459 Na–Ca clinozoisite temperatures vary from 90 to 323 °C, with an average of 250 °C, a median of 252 °C, and a standard deviation of 44 °C. The error on the Na–Ca clinozoisite temperatures ranges between 0 and 30 °C, with a mean of 6.5 °C, a median of 5.0 °C, and a standard deviation of 5.0 °C.

The 169 Na–Ca wairakite temperatures range from 173 to 335 °C, with mean and median of 261 °C and standard deviation of 30 °C. The error on Na–Ca wairakite temperatures varies between 0 and 37 °C, with an average of 7.8 °C, a median of 8.0 °C, and a standard deviation of 5.6 °C.

The 63 Na–Ca laumontite temperatures vary from 155 to 322 °C, with an average of 235 °C, a median of 239 °C, and a standard deviation of 24 °C. The error on Na–Ca laumontite temperatures ranges between 0 and 21 °C, with a mean of 5.8 °C, a median of 5.0 °C, and a standard deviation of 4.7 °C.

The 15 Na–Ca prehnite temperatures range from 123 to 263 °C, with a mean of 176 °C, a median of 147 °C, and a standard deviation of 50 °C. The error on Na–Ca prehnite temperatures varies between 8 and 25 °C, with an average of 16.5 °C, a median of 17.0 °C, and a standard deviation of 4.4 °C.

The average and median values of the K–Ca clinozoisite temperatures agree with the average and median values of the Na–Ca clinozoisite temperatures within a few degrees. Similarly, there is a good agreement between the average and median values of the K–Ca and Na–Ca temperatures for wairakite and laumontite as well. In contrast, the average and median values of the K–Ca prehnite temperatures are at variance with the mean and median values of the Na–Ca prehnite temperatures. This discrepancy is due, at least partly, to the different number of cases, 51 for the K–Ca prehnite temperatures versus 15 for the Na–Ca prehnite temperatures.

The higher number of adopted K–Ca and Na–Ca clinozoisite temperatures compared to the other Ca–Al silicate temperatures is in accordance with the widespread occurrence of hydrothermal epidote in active geothermal systems. Moreover, the K–Ca and Na–Ca laumontite, clinozoisite, and wairakite temperatures are in satisfactory agreement with the distinct distribution of these three hydrothermal minerals in active geothermal systems, where the stable Ca–Al-silicate is wairakite or epidote or prehnite at high temperatures, typically 200–300 °C, and laumontite at lower temperatures, as already recalled in Chaps. 4 and 5.

The errors on K–Ca and Na–Ca temperatures are partly explained by the deviation of the activities of relevant minerals from the average values, considering that deviations of $+1\sigma$ and -1σ from the mean value of the pertinent activity term cause uncertainties of 3.8, 2.7, 1.8, and 9.6 °C in the K–Ca temperatures of clinozoisite, wairakite, laumontite, and prehnite, respectively, whereas the uncertainties of this type on the corresponding Na–Ca temperatures are 5.3, 3.4, 5.0, and 17.9 °C, respectively.

Finally, the identification of the Ca–Al-silicate in equilibrium with each reservoir liquid may provide a qualitative indication on well permeability. In fact, according to Reyes (1990), wairakite is an indicator of high permeability, whereas prehnite and laumontite (if abundant) are indicators of poor permeability. Prehnite apparently requires little flow of geothermal fluids through the rocks to form as it appears to recrystallize easily, with increase in temperature, from the primary Fe–Mg minerals, such as pyroxene (Reyes 1990).

8.8.2 CO_2 Fugacities Given by the Theoretical, Activity-Based K–Ca and Na–Ca Calcite f_{CO_2}-Indicators and Related Uncertainties

The CO_2 fugacity was computed by means of the theoretical K–Ca and Na–Ca calcite f_{CO_2}-indicators for 283 reservoir liquids coming from the geothermal fields of Krafla, Namafjall, Nesjavellir, Hellisheidi, Dixie Valley, Long Valley, Valles, Coso, Salton Sea, Los Azufres, Berlin, Mori-Nigorikawa, Uenotai, Oku-aizu, Bacon Manito, Tongonan (Mahiao and Malitbog sectors), Mahanagdong, Alto Peak, Palin-pinon, Ngawha, Kawerau, Orakeikorako, Mokai, Broadlands, Rotokawa, Yang-bajing, Kizildere, Aluto-Langano, Olkaria, Bagnore, Latera, Mofete, and Ribeira Grande. All these reservoir liquids are presumably in equilibrium with calcite. Since the CO_2 fugacities given by the theoretical K–Ca and Na–Ca calcite f_{CO_2}-indicators are practically equal (see Sect. 8.7), the average of the two values was taken and plotted against both:

1. the CO_2 fugacities calculated by means of speciation calculations (Figs. 8.14a, 8.15a, 8.16a, and 8.17a), that is combining the analyses of the liquid and vapor phases separated at known pressure, temperature conditions, usually using the computer program WATCH, and
2. the CO_2 fugacities computed using the K–Ca f_{CO_2}-indicator of Giggenbach (1984; Figs. 8.14b, 8.15b, 8.16b, and 8.17b), which is discussed in Sect. 5.5.

The reasons of the deviations observed in these diagrams are discussed in Sect. 5.5.2 and are disregarded here to avoid unnecessary repetitions. The absolute value of the difference between the CO_2 fugacities given by the theoretical K–Ca
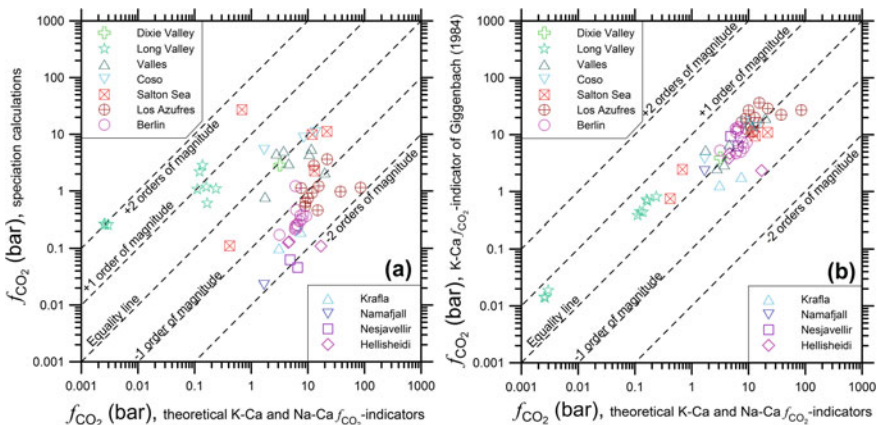
Fig. 8.14 Log-log diagram of the average CO_2 fugacity given by the theoretical K–Ca and Na–Ca calcite f_{CO_2}-indicators versus **a** the CO_2 fugacity obtained from speciation calculations and **b** the CO_2 fugacity computed using the K–Ca f_{CO_2}-indicator of Giggenbach (1984) for the geothermal fields of Iceland and Northern-Central America
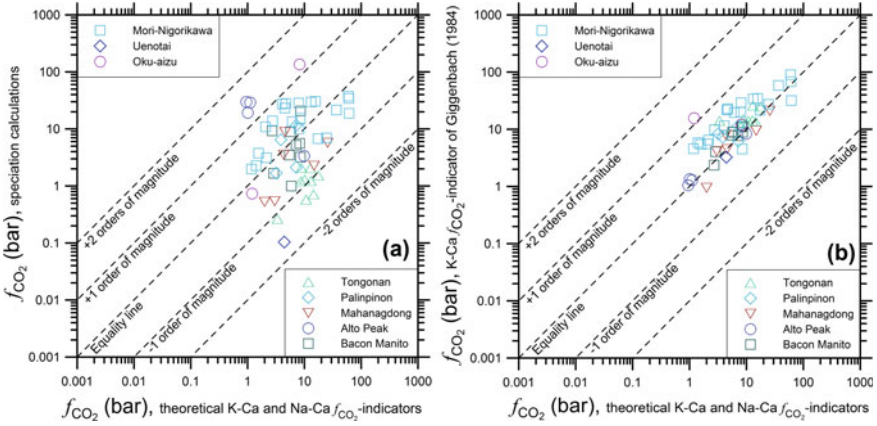
Fig. 8.15 Log-log diagram of the average CO_2 fugacity given by the theoretical K–Ca and Na–Ca calcite f_{CO_2}-indicators versus **a** the CO_2 fugacity obtained from speciation calculations and **b** the CO_2 fugacity computed using the K–Ca f_{CO_2}-indicator of Giggenbach (1984) for the geothermal fields of Japan and the Philippines
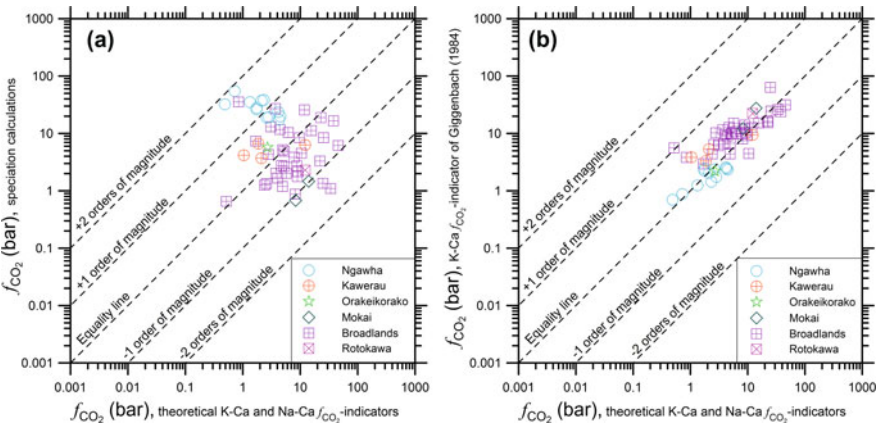
Fig. 8.16 Log-log diagram of the average CO_2 fugacity given by the theoretical K–Ca and Na–Ca calcite f_{CO_2}-indicators versus **a** the CO_2 fugacity obtained from speciation calculations and **b** the CO_2 fugacity computed using the K–Ca f_{CO_2}-indicator of Giggenbach (1984) for the geothermal fields of New Zealand

and Na–Ca calcite f_{CO_2}-indicators and the CO_2 fugacities calculated by means of speciation calculations ranges between 0.0093 and 2.19 log-units, with an average of 0.78 log-units, a median of 0.66 log-units, and a standard deviation of 0.54 log-units. The absolute value of these differences is ≤0.50 log-units in 110 cases (38.9% of the total), >0.50 and ≤1.00 log-units in 78 cases (27.6% of the total), >1.00 and ≤1.50 log-units in 63 cases (22.3% of the total) >1.50 and ≤2.00 log-units in 28 cases (9.9% of the total), and >2.00 log-units in 4 cases (1.4% of the total).
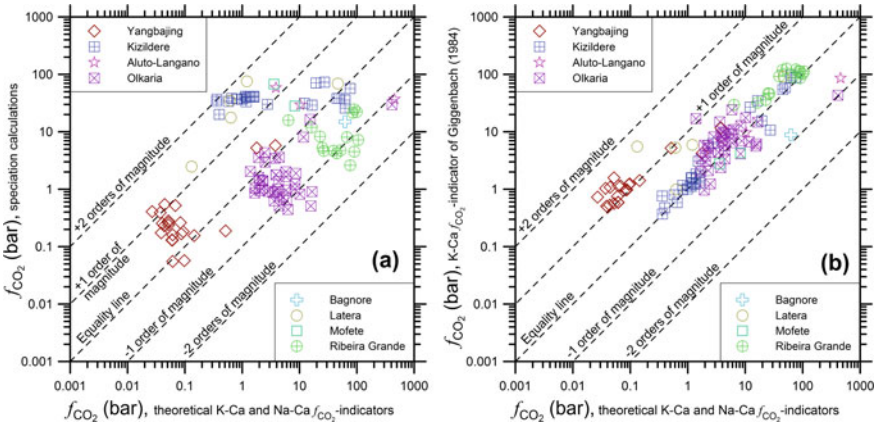
Fig. 8.17 Log-log diagram of the average CO_2 fugacity given by the theoretical K–Ca and Na–Ca calcite f_{CO_2}-indicators versus **a** the CO_2 fugacity obtained from speciation calculations and **b** the CO_2 fugacity computed using the K–Ca f_{CO_2}-indicator of Giggenbach (1984) for the miscellaneous geothermal fields

The absolute value of the difference between the CO_2 fugacities given by the theoretical K–Ca and Na–Ca calcite f_{CO_2}-indicators and the CO_2 fugacities computed using the K–Ca f_{CO_2}-indicator of Giggenbach (1984) varies between 0.00029 and 1.62 log-units, with a mean of 0.33 log-units, a median of 0.24 log-units, and a standard deviation of 0.32 log-units. The absolute value of these differences is ≤0.50 log-units in 228 cases (80.6% of the total), >0.50 and ≤1.00 log-units in 34 cases (12.0% of the total), >1.00 and ≤1.50 log-units in 20 cases (7.1% of the total), and >1.50 log-units in 1 case (0.4% of the total).

The satisfactory agreement between the CO_2 fugacities calculated by means of the theoretical K–Ca and Na–Ca calcite f_{CO_2}-indicators and the CO_2 fugacities given by the K–Ca f_{CO_2}-indicator of Giggenbach (1984) is not surprising. In fact, the theoretical K–Ca calcite f_{CO_2}-indicator developed in this work is an improved version of the K–Ca f_{CO_2}-indicator of Giggenbach (1984). This improvement is mainly due to the use of the activities of K^+ and Ca^{2+} ions instead of the total concentrations of K and Ca, respectively.

Following the rigorous approach developed here, the CO_2 fugacities given by the theoretical K–Ca and Na–Ca calcite f_{CO_2}-indicators were considered reliable if higher than the maximum CO_2 fugacity of Ca–Al-silicate/calcite coexistence. However, the theoretical K–Ca and Na–Ca calcite f_{CO_2}-indicators can be probably used even if the CO_2 fugacities obtained by means of the theoretical K–Ca and Na–Ca calcite f_{CO_2}-indicators are somewhat lower than the maximum CO_2 fugacity of Ca–Al-silicate/calcite coexistence, provided that differences are not too large.

8.9   Final Considerations on the Activity-Based Theoretical K–Ca and Na–Ca Geoindicators

The activity-based theoretical K–Ca and Na–Ca geothermometers developed in this work are based on exchange reactions involving laumontite, clinozoisite, prehnite, and wairakite, whereas the activity-based theoretical K–Ca and Na–Ca f_{CO_2}-indicators implemented here are built on reactions including calcite. Adularia participates to the exchange reactions controlling all the theoretical K–Ca geothermometers and f_{CO_2}-indicators and some Na–Ca geothermometers and f_{CO_2}-indicators. Consequently, these functions involve the ordering parameter of hydrothermal adularia in hypothetical equilibrium with each reservoir liquid of interest, which is obtained from the Na–K activity-ratio and the reservoir temperature (see Chap. 6).

The theoretical K–Ca and Na–Ca geoindicators were tested with about one thousand reservoir liquids. The theoretical K–Ca geothermometers reproduce aquifer temperature with an average error of 3.8 °C and the error is lower than 10 °C in 97.3% of the cases. The theoretical Na–Ca geothermometers reproduce aquifer temperature with an average error of 6.9 °C and the error is less than 15 °C in 93.5% of the cases.

The CO_2 fugacities given by theoretical K–Ca and Na–Ca f_{CO_2}-indicators match satisfactorily the CO_2 fugacities given by the K–Ca f_{CO_2}-indicator of Giggenbach (1984), with an absolute deviation of 0.33 log-units on average, whereas the agreement with the CO_2 fugacities computed by means of speciation calculations is less good, with an absolute deviation of 0.78 log-units on average.

These good performances of the activity-based theoretical K–Ca and Na–Ca geothermometers, and to a lower extent of the f_{CO_2}-indicators as well, are expected because the activities of the Ca-bearing endmembers in relevant hydrothermal minerals from active geothermal systems (i.e., laumontite in laumontite/alkali-laumontite, clinozoisite in clinozoisite/epidote, prehnite in prehnite/ferri-prehnite, wairakite in wairakite/analcime, and calcite in calcite-rich trigonal carbonates) and the activity of muscovite in hydrothermal illites from active geothermal systems do not deviate too much from the average values and average activities do not depart too much from unity (see Chap. 4 and Sect. 8.2).[1]

In addition to these good performances in terms of computed aquifer temperatures and CO_2 fugacities, the theoretical K–Ca and Na–Ca geothermometers and f_{CO_2}-indicators allow one to identify the Ca-bearing solid phase in equilibrium with each reservoir liquid, either a Ca–Al-silicate (laumontite or clinozoisite or prehnite or wairakite) or calcite. This indication represents a significant step forward with respect to the results of the traditional K–Ca and Na–Ca geoindicators and is probably more reliable than the outcomes of multicomponent chemical geothermometry (see Sect. 5.9), being marginally affected by pH and Al concentration. Finally, the identification of the Ca–Al-silicate in equilibrium with each reservoir liquid may

---

[1]Following the same line of reasoning, K–Ca and Na–Ca theoretical geoindicators based on the exchange reactions involving grossular were not developed because grossular activity in 190 garnet solid solutions from active geothermal systems ranges from $<2.27 \cdot 10^{-7}$ (in 22 cases) to 0.674, with average of 0.127, median of 0.0142, and standard deviation of 0.179.

provide a qualitative indication on well permeability. In fact, wairakite is an indicator of high permeability, whereas prehnite and laumontite (if abundant) are indicators of poor permeability (Reyes 1990).

It is advisable, not to say it is mandatory, to complement the application of the theoretical K–Ca and Na–Ca geothermometers and f_{CO_2}-indicators derived in this book with the plots of the K^2/Ca log-activity ratio versus the absolute temperature reciprocal, the Na^2/Ca log-activity ratio versus the absolute temperature inverse (see Sect. 8.6) and the CO_2 fugacity versus the absolute temperature reciprocal (see Sect. 8.7), all providing useful overviews through the eyeball comparison of all the aqueous solutions of interest with the theoretical geoindicators.

References

Arnórsson S (1985) The use of mixing models and chemical geothermometers for estimating underground temperatures in geothermal systems. J Volcanol Geotherm Res 23:299–335

Arnórsson S, Gunnlaugsson E (1985) New gas geothermometers for geothermal exploration—calibration and application. Geochim Cosmochim Acta 49:1307–1325

Arnórsson S, Gunnlaugsson E, Svavarsson H (1983) The chemistry of geothermal waters in Iceland. III. Chemical geothermometry in geothermal investigations. Geochim Cosmochim Acta 47:567–577

Chiodini G, Cioni R, Guidi M, Marini L (1991) Chemical geothermometry and geobarometry in hydrothermal aqueous solutions: a theoretical investigation based on a mineral-solution equilibrium model. Geochim Cosmochim Acta 55:2709–2727

Ellis AJ (1970) Quantitative interpretation of chemical characteristics of hydrothermal systems. Geothermics 2:516–528

Giggenbach WF (1981) Geothermal mineral equilibria. Geochim Cosmochim Acta 45:393–410

Giggenbach WF (1982) "Geothermal mineral equilibria". Reply to a comment by M.A. Grant. Geochim Cosmochim Acta 46:2681–2683

Giggenbach WF (1984) Mass transfer in hydrothermal alterations systems. Geochim Cosmochim Acta 48:2693–2711

Giggenbach WF (1988) Geothermal solute equilibria. Derivation of Na-K-Mg-Ca geoindicators. Geochim Cosmochim Acta 52:2749–2765

Grant MA (1982) On the lack of a unique relation between CO_2 partial pressure and temperature in geothermal system. Comment on "Geothermal mineral equilibria" by W.F. Giggenbach. Geochim Cosmochim Acta 46:2677–2680

Kacandes GH, Grandstaff DE (1989) Differences between geothermal and experimentally derived fluids: how well do hydrothermal experiments model the composition of geothermal reservoir fluids? Geochim Cosmochim Acta 53:343–358

Mahon WAJ, McDowell GD, Finlayson JB (1980) Carbon dioxide: its role in geothermal systems. New Zeal J Sci 23:133–148

Reyes AG (1990) Petrology of Philippine geothermal systems and the application of alteration mineralogy to their assessment. J Volcanol Geotherm Res 43:279–309

Truesdell AH, Nakanishi S (2005) Chemistry of neutral and acid production fluids from the Onikobe geothermal field, Miyagi Prefecture, Honshu, Japan. In: Use of isotope techniques to trace the origin of acidic fluids in geothermal systems. IAEA-TECDOC-1448, pp 169–193